THE UNIVERSITY *of* EDINBURGH

Edinburgh Research Explorer

Measurement of CP violation parameters and polarisation fractions in $ {\mathrm{B}}_{\mathrm{s}}^0\to \mathrm{J}/\psi {\overline{\mathrm{K}}}^{\ast 0} $ decays

Measurement of *CP* violation parameters and polarisation fractions in $B_s^0 \rightarrow J/\psi\, \overline{K}^{*0}$ decays

The LHCb collaboration

E-mail: carlos.vazquez@cern.ch

ABSTRACT: The first measurement of *CP* asymmetries in the decay $B_s^0 \rightarrow J/\psi \, \overline{K}^*(892)^0$ and an updated measurement of its branching fraction and polarisation fractions are presented. The results are obtained using data corresponding to an integrated luminosity of $3.0\,\mathrm{fb}^{-1}$ of proton-proton collisions recorded with the LHCb detector at centre-of-mass energies of 7 and 8 TeV. Together with constraints from $B^0 \rightarrow J/\psi \, \rho^0$, the results are used to constrain additional contributions due to penguin diagrams in the *CP*-violating phase ϕ_s, measured through B_s^0 decays to charmonium.

Contents

1 Introduction

The *CP*-violating phase ϕ_s arises in the interference between the amplitudes of B_s^0 mesons decaying via $b \to c\bar{c}s$ transitions to *CP* eigenstates directly and those decaying after oscillation. The phase ϕ_s can be measured using the decay $B_s^0 \to J/\psi\phi$. Within the Standard Model (SM), and ignoring penguin contributions to the decay, ϕ_s is predicted to be $-2\beta_s$, with $\beta_s \equiv \arg(-V_{cb}V_{cs}^*/V_{tb}V_{ts}^*)$, where V_{ij} are elements of the CKM matrix [1]. The phase ϕ_s is a sensitive probe of dynamics beyond the SM (BSM) since it has a very small theoretical uncertainty and BSM processes can contribute to B_s^0-$\bar{B}_s^0$ mixing [2–5]. Global fits to experimental data, excluding the direct measurements of ϕ_s, give $-2\beta_s = -0.0363 \pm 0.0013\,\text{rad}$ [6]. The current world average value is $\phi_s = -0.015 \pm 0.035\,\text{rad}$ [7], dominated by the LHCb measurement reported in ref. [8]. In the SM expectation of ϕ_s [6], additional contributions to the leading $b \to c\bar{c}s$ tree Feynman diagram, as shown in figure 1, are assumed to be negligible. However, the shift in ϕ_s due to these contributions, called hereafter "penguin pollution", is difficult to compute due to the non-perturbative nature of the quantum chromodynamics (QCD) processes involved. This penguin pollution must be measured or limited before using the ϕ_s measurement in searches for BSM effects, since a shift in this phase caused by penguin diagrams is possible. Various methods to address this problem have been proposed [9–14], and LHCb has recently published upper limits on the size of the penguin-induced phase shift using $B^0 \to J/\psi\rho^0$ decays [15].

Tree and penguin diagrams contributing to both $B_s^0 \to J/\psi\phi$ and $B_s^0 \to J/\psi\bar{K}^{*0}$ decays are shown in figure 1. In this paper, the penguin pollution in ϕ_s is investigated using $B_s^0 \to J/\psi\bar{K}^{*0}$ decays,[1] with $J/\psi \to \mu^+\mu^-$ and $\bar{K}^{*0} \to K^-\pi^+$, following the method first proposed in ref. [9] for the $B^0 \to J/\psi\rho^0$ decay and later also discussed for the $B_s^0 \to J/\psi\bar{K}^{*0}$ decay in refs. [11, 13]. This approach requires the measurement of the branching fraction, direct *CP* asymmetries, and polarisation fractions of the $B_s^0 \to J/\psi\bar{K}^{*0}$ decay. The measurements use data from proton-proton (pp) collisions recorded with the LHCb detector corresponding to $3.0\,\text{fb}^{-1}$ of integrated luminosity, of which $1.0\,(2.0)\,\text{fb}^{-1}$ was collected in 2011 (2012) at a centre-of-mass energy of 7 (8) TeV. The LHCb collaboration previously reported a measurement of the branching fraction and the polarisation fractions using data corresponding to $0.37\,\text{fb}^{-1}$ of integrated luminosity [16].

The paper is organised as follows: a description of the LHCb detector, reconstruction and simulation software is given in section 2, the selection of the $B_s^0 \to J/\psi\bar{K}^{*0}$ signal candidates and the $B^0 \to J/\psi K^{*0}$ control channel are presented in section 3 and the treatment of background in section 4. The $J/\psi K^-\pi^+$ invariant mass fit is detailed in section 5. The angular analysis and *CP* asymmetry measurements, both performed on weighted distributions where the background is statistically subtracted using the *sPlot* technique [17], are detailed in section 6. The measurement of the branching fraction is explained in section 7. The evaluation of systematic uncertainties is described in section 8 along with the results, and in section 9 constraints on the penguin pollution are evaluated and discussed.

---

[1]Charge conjugation is implicit throughout this paper, unless otherwise specified.
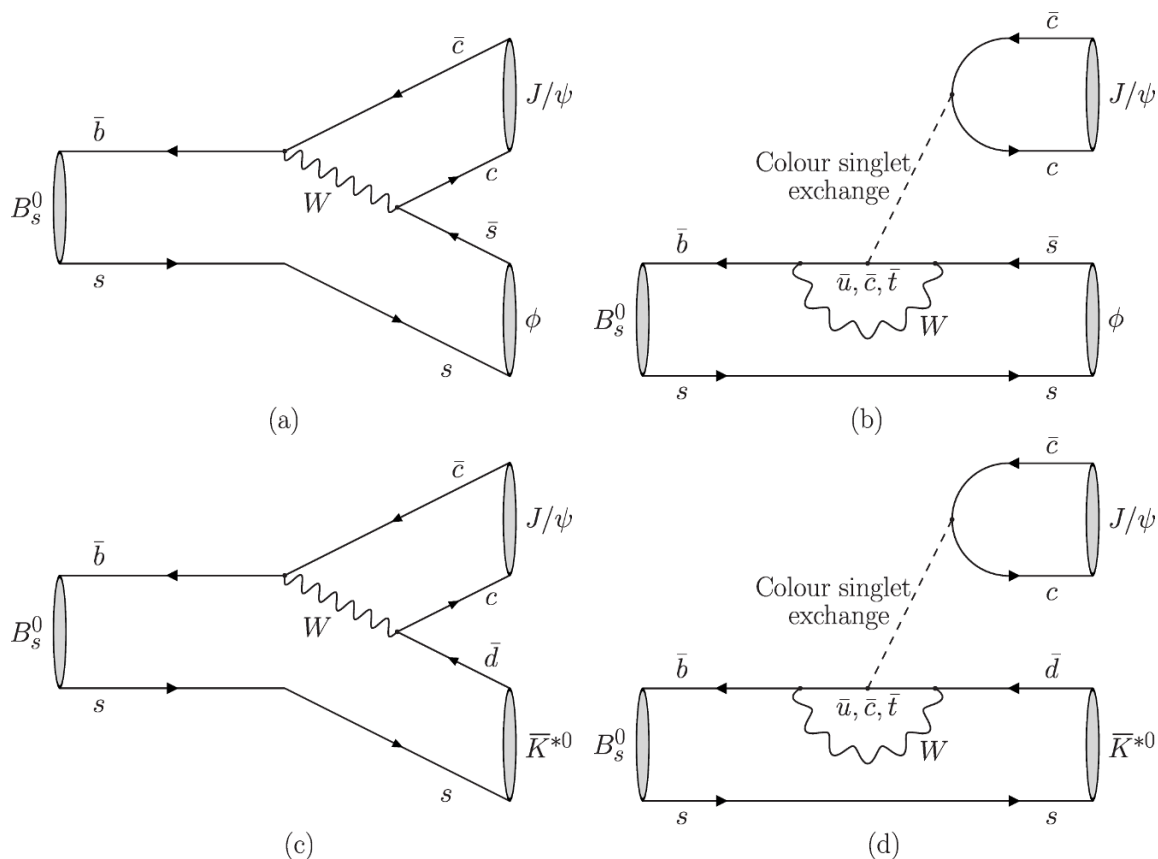
Figure 1. Decay topologies contributing to the $B_s^0 \rightarrow J/\psi\,\phi$ channel (a, b) and $B_s^0 \rightarrow J/\psi\,\overline{K}^{*0}$ channel (c, d). The tree diagrams (a, c) are shown on the left and the penguin diagrams (b, d) on the right.

2 Experimental setup

The LHCb detector [18, 19] is a single-arm forward spectrometer covering the pseudo-rapidity range $2 < \eta < 5$, designed for the study of particles containing b or c quarks. The detector includes a high-precision tracking system consisting of a silicon-strip vertex detector surrounding the pp interaction region, a large-area silicon-strip detector located upstream of a dipole magnet with a bending power of about $4\,\mathrm{Tm}$, and three stations of silicon-strip detectors and straw drift tubes placed downstream of the magnet. The tracking system provides a measurement of momentum, p, of charged particles with a relative uncertainty that varies from 0.5% at low momentum to 1.0% at $200\,\mathrm{GeV}/c$. The minimum distance of a track to a primary vertex, the impact parameter, is measured with a resolution of $(15+29/p_{\mathrm{T}})\,\mu\mathrm{m}$, where p_{T} is the component of the momentum transverse to the beam, in GeV/c. Different types of charged hadrons are distinguished using information from two ring-imaging Cherenkov detectors. Photons, electrons and hadrons are identified by a calorimeter system consisting of scintillating-pad and preshower detectors, an electromagnetic calorimeter and a hadronic calorimeter. Muons are identified by a system composed of alternating layers of iron and multiwire proportional chambers.

The online event selection is performed by a trigger, which consists of a hardware stage, based on information from the calorimeter and muon systems, followed by a software stage, which applies a full event reconstruction. In this analysis, candidates are first required to pass the hardware trigger, which selects muons with a transverse momentum $p_{\mathrm{T}} >$ 1.48 GeV/c in the 7 TeV data or $p_{\mathrm{T}} > 1.76$ GeV/c in the 8 TeV data. In the subsequent software trigger, at least one of the final-state particles is required to have both $p_{\mathrm{T}} >$ 0.8 GeV/c and impact parameter larger than 100 μm with respect to all of the primary pp interaction vertices (PVs) in the event. Finally, the tracks of two or more of the final-state particles are required to form a vertex that is significantly displaced from any PV. Further selection requirements are applied offline in order to increase the signal purity.

In the simulation, pp collisions are generated using PYTHIA [20, 21] with a specific LHCb configuration [22]. Decays of hadronic particles are described by EVTGEN [23], in which final-state radiation is generated using PHOTOS [24]. The interaction of the generated particles with the detector, and its response, are implemented using the GEANT4 toolkit [25, 26] as described in ref. [27].

3 Event selection

The selection of $B_s^0 \to J/\psi \, \overline{K}^{*0}$ candidates consists of two steps: a preselection consisting of discrete cuts, followed by a specific requirement on a boosted decision tree with gradient boosting (BDTG) [28, 29] to suppress combinatorial background. All charged particles are required to have a transverse momentum in excess of 0.5 GeV/c^2 and to be positively identified as muons, kaons or pions. The tracks are fitted to a common vertex which is required to be of good quality and significantly displaced from any PV in the event. The flight direction can be described as a vector between the B_s^0 production and decay vertices; the cosine of the angle between this vector and the B_s^0 momentum vector is required to be greater than 0.999. Reconstructed invariant masses of the J/ψ and $\overline{K}^{*0}$ candidates are required to be in the ranges $2947 < m_{\mu^+\mu^-} < 3247$ MeV/c^2 and $826 < m_{K^-\pi^+} <$ 966 MeV/c^2. The B_s^0 invariant mass is reconstructed by constraining the J/ψ candidate to its nominal mass [30], and is required to be in the range $5150 < m_{J/\psi K^-\pi^+} < 5650$ MeV/c^2.

The training of the BDTG is performed independently for 2011 and 2012 data, using information from the B_s^0 candidates: time of flight, transverse momentum, impact parameter with respect to the production vertex and χ^2 of the decay vertex fit. The data sample used to train the BDTG uses less stringent particle identification requirements. When training the BDTG, simulated $B_s^0 \to J/\psi \, \overline{K}^{*0}$ events are used to represent the signal, while candidates reconstructed from data events with $J/\psi K^-\pi^+$ invariant mass above 5401 MeV/c^2 are used to represent the background. The optimal threshold for the BDTG is chosen independently for 2011 and 2012 data and maximises the effective signal yield.

4 Treatment of peaking backgrounds

After the suppression of most background with particle identification criteria, simulations show residual contributions from the backgrounds $\Lambda_b^0 \to J/\psi \, pK^-$, $B_s^0 \to J/\psi \, K^+K^-$,

$B_s^0 \to J/\psi \pi^+ \pi^-$, and $B^0 \to J/\psi \pi^+ \pi^-$. The invariant mass distributions of misidentified $B^0 \to J/\psi \pi^+ \pi^-$ and $B_s^0 \to J/\psi \pi^+ \pi^-$ events peak near the $B_s^0 \to J/\psi K^- \pi^+$ signal peak due to the effect of a wrong-mass hypothesis, and the misidentified $B_s^0 \to J/\psi K^+ K^-$ candidates are located in the vicinity of the $B^0 \to J/\psi K^+ \pi^-$ signal peak. It is therefore not possible to separate such background from signal using information based solely on the invariant mass of the $J/\psi K^- \pi^+$ system. Moreover the shape of the reflected invariant mass distribution is sensitive to the daughter particles momenta. Due to these correlations it is difficult to add the b-hadron to $J/\psi h^+ h^-$ (where h is either a pion, a kaon or a proton) misidentified backgrounds as extra modes to the fit to the invariant mass distribution. Instead, simulated events are added to the data sample with negative weights in order to cancel the contribution from those peaking backgrounds, as done previously in ref. [8]. Simulated b-hadron to $J/\psi h^+ h^-$ events are generated using a phase-space model, and then weighted on an event-by-event basis using the latest amplitude analyses of the decays $\Lambda_b^0 \to J/\psi p K^-$ [31], $B_s^0 \to J/\psi K^+ K^-$ [32], $B_s^0 \to J/\psi \pi^+ \pi^-$ [33], and $B^0 \to J/\psi \pi^+ \pi^-$ [34]. The sum of weights of each decay mode is normalised such that the injected simulated events cancel out the expected yield in data of the specific background decay mode.

In addition to $\Lambda_b^0 \to J/\psi p K^-$ and $B \to J/\psi h^+ h^-$ decays, background from $\Lambda_b^0 \to J/\psi p \pi^-$ is also expected. However, in ref. [35] a full amplitude analysis was not performed. For this reason, as well as the fact that the Λ_b^0 decays have broad mass distributions, the contribution is explicitly included in the mass fit described in the next section. Expected yields for both $B \to J/\psi h^+ h^-$ and $\Lambda_b^0 \to J/\psi p h^-$ background decays are given in table 1.

5   Fit to the invariant mass distribution

After adding simulated $B^0 \to J/\psi \pi^+ \pi^-$, $B_s^0 \to J/\psi \pi^+ \pi^-$, $B_s^0 \to J/\psi K^+ K^-$, and $\Lambda_b^0 \to J/\psi p K^-$ events with negative weights, the remaining sample consists of $B^0 \to J/\psi K^+ \pi^-$, $B_s^0 \to J/\psi K^- \pi^+$, $\Lambda_b^0 \to J/\psi p \pi^-$ decays, and combinatorial background. These four modes are statistically disentangled through a fit to the $J/\psi K^- \pi^+$ invariant mass. The combinatorial background is described by an exponential distribution, the $\Lambda_b^0 \to J/\psi p \pi^-$ decay by the Amoroso distribution [36] and the B^0 and B_s^0 signals by the double-sided Hypatia distribution [37],

$$I(m, \mu, \sigma, \lambda, \zeta, \beta, a_1, a_2, n_1, n_2) \propto$$
$$\begin{cases} \frac{A}{(B+m-\mu)^{n_1}} & \text{if } m - \mu < -a_1\sigma, \\ \frac{C}{(D+m-\mu)^{n_2}} & \text{if } m - \mu > a_2\sigma, \\ \left((m-\mu)^2 + \delta^2\right)^{\frac{1}{2}\lambda - \frac{1}{4}} e^{\beta(m-\mu)} K_{\lambda - \frac{1}{2}}\left(\alpha\sqrt{(m-\mu)^2 + \delta^2}\right) & \text{otherwise}, \end{cases}$$
$$(5.1)$$

where $K_\nu(z)$ is the modified Bessel function of the second kind, $\delta \equiv \sigma\sqrt{\frac{\zeta K_\lambda(\zeta)}{K_{\lambda+1}(\zeta)}}$, $\alpha \equiv \frac{1}{\sigma}\sqrt{\frac{\zeta K_{\lambda+1}(\zeta)}{K_\lambda(\zeta)}}$, and A, B, C, D are obtained by imposing continuity and differentiability. This function is chosen because the event-by-event uncertainty on the mass has a dependence on the particle momenta. The estimate of the number of $B^0 \to J/\psi K^+ \pi^-$ decays lying

Background sources	2011 data	2012 data
$B^0 \to J/\psi \pi^+\pi^-$	51 ± 10	115 ± 23
$B_s^0 \to J/\psi \pi^+\pi^-$	9.3 ± 2.1	25.0 ± 5.4
$B_s^0 \to J/\psi K^+K^-$	10.1 ± 2.3	19.2 ± 4.0
$\Lambda_b^0 \to J/\psi pK^-$	36 ± 17	90 ± 43
$\Lambda_b^0 \to J/\psi p\pi^-$	13.8 ± 5.3	27.3 ± 9.0

Table 1. Expected yields of each background component in the signal mass range.

under the B_s^0 peak is very sensitive to the modelling of the tails of the B^0 peak. The fitted fraction is in good agreement with the estimate from simulation.

In the fit to data, the mean and resolution parameters of both the B_s^0 and B^0 Hypatia functions are free to vary. All the remaining parameters, namely λ, a_1, n_1, a_2 and n_2, are fixed to values determined from fits to B_s^0 and B^0 simulated events. All the $\Lambda_b^0 \to J/\psi p\pi^-$ shape parameters are fixed to values obtained from fits to simulated $\Lambda_b^0 \to J/\psi p\pi^-$ events, while the exponent of the combinatorial background is free to vary.

Due to the small expected yield of $\Lambda_b^0 \to J/\psi p\pi^-$ decays compared to those of the other modes determined in the fit to data, and to the broad distribution of $\Lambda_b^0 \to J/\psi p\pi^-$ decays across the $J/\psi K^-\pi^+$ invariant mass spectrum, its yield is included in the fit as a Gaussian constraint using the expected number of events and its uncertainties, as shown in table 1.

From studies of simulated (MC) samples, it is found that the resolution of B_s^0 and B^0 mass peaks depends on both $m_{K^-\pi^+}$ and $\cos(\theta_\mu)$, where θ_μ is one of the helicity angles used in the angular analysis as defined in section 6. The fit to the $J/\psi K^-\pi^+$ invariant mass spectrum, including the evaluation of the $sWeights$, is performed separately in twenty bins, corresponding to four $m_{K^-\pi^+}$ bins of $35\,\mathrm{MeV}/c^2$ width, and five equal bins in $\cos(\theta_\mu)$. The overall B_s^0 and B^0 yields are obtained from the sum of yields in the twenty bins, giving

$$N_{B^0} = 208656 \pm 462\,(\mathrm{stat})^{+78}_{-76}\,(\mathrm{syst})\,, \tag{5.2}$$

$$N_{B_s^0} = 1808 \pm 51\,(\mathrm{stat})^{+38}_{-33}\,(\mathrm{syst})\,, \tag{5.3}$$

where the statistical uncertainties are obtained from the quadratic sum of the uncertainties determined in each of the individual fits. Systematic uncertainties are discussed in section 8. The correlation between the B^0 and B_s^0 yields in each bin are found to be smaller than 4%. The ratio of the B_s^0 and B^0 yields is found to be $N_{B_s^0}/N_{B^0} = (8.66 \pm 0.24(\mathrm{stat})^{+0.18}_{-0.16}(\mathrm{syst})) \times 10^{-3}$. Figure 2 shows the sum of the fit results for each bin, overlaid on the $J/\psi K^-\pi^+$ mass spectrum for the selected data sample.

6 Angular analysis

6.1 Angular formalism

This analysis uses the decay angles defined in the helicity basis. The helicity angles are denoted by $(\theta_K, \theta_\mu, \varphi_h)$, as shown in figure 3. The polar angle θ_K (θ_μ) is the angle between
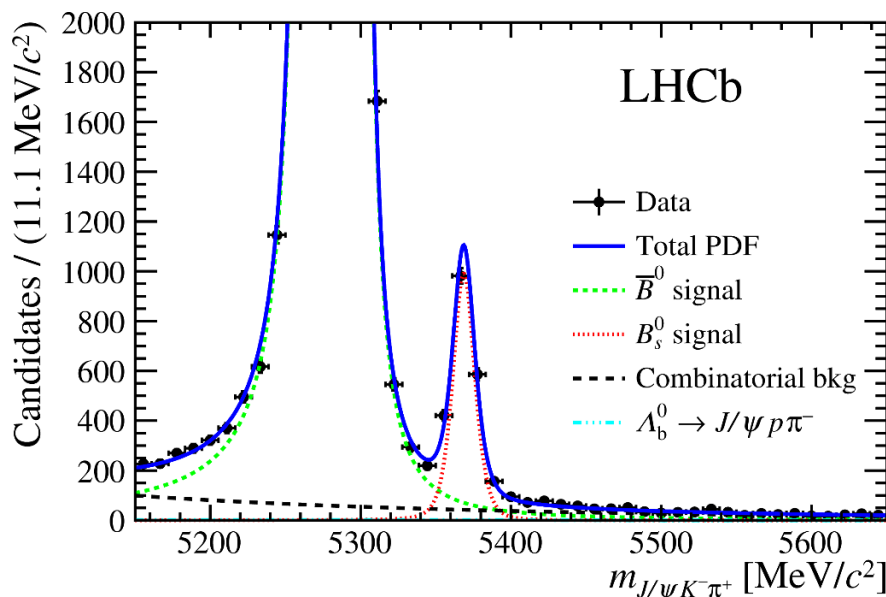
Figure 2. The $J/\psi K^-\pi^+$ invariant mass distribution with the sum of the fit projections in the 20 $m_{K^-\pi^+}$ and $\cos(\theta_\mu)$ bins. Points with error bars show the data. The projection of the fit result is represented by the solid blue line, and the contributions from the different components are detailed in the legend. At this scale the contribution of the $\Lambda_b^0 \to J/\psi p\pi^-$ is barely visible. All the other peaking background components are subtracted as described in the text.
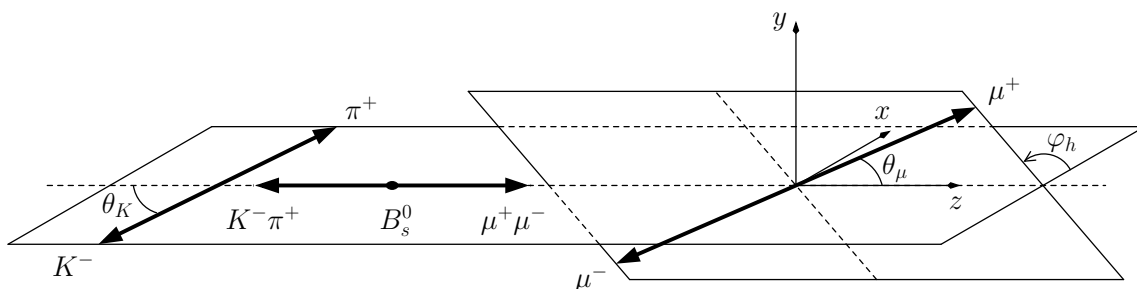
Figure 3. Representation of helicity angles as discussed in the text.

the kaon (μ^+) momentum and the direction opposite to the B_s^0 momentum in the $K^-\pi^+$ ($\mu^+\mu^-$) centre-of-mass system. The azimuthal angle between the $K^-\pi^+$ and $\mu^+\mu^-$ decay planes is φ_h. The definitions are the same for B_s^0 or $\overline{B}_s^0$ decays. They are also the same for $B^0 \to J/\psi K^{*0}$ decays.

The shape of the angular distribution of $B_s^0 \to J/\psi \overline{K}^{*0}$ decays is given by ref. [38],

$$\frac{\mathrm{d}\Gamma(\theta_K, \theta_\mu, \varphi_h)}{\mathrm{d}\Omega} \propto \sum_{\alpha_\mu = \pm 1} \left| \sum_{\lambda, J}^{|\lambda| < J} \sqrt{\frac{2J+1}{4\pi}} \mathcal{H}_\lambda^J e^{-i\lambda\varphi_h} d^1_{\lambda,\alpha_\mu}(\theta_\mu) d^1_{-\lambda,0}(\theta_K) \right|^2, \qquad (6.1)$$

where $\lambda = 0, \pm 1$ is the J/ψ helicity, $\alpha_\mu = \pm 1$ is the helicity difference between the muons, J is the spin of the $K^-\pi^+$ system, $\mathcal{H}$ are the helicity amplitudes, and d are the small Wigner matrices.

The helicity amplitudes are rotated into transversity amplitudes, which correspond to final P eigenstates,

$$A_{\text{S}} = \mathcal{H}_0^0 \,, \tag{6.2}$$

$$A_0 = \mathcal{H}_0^1 \,, \tag{6.3}$$

$$A_\parallel = \frac{1}{\sqrt{2}}(\mathcal{H}_+^1 + \mathcal{H}_-^1) \,, \tag{6.4}$$

$$A_\perp = \frac{1}{\sqrt{2}}(\mathcal{H}_+^1 - \mathcal{H}_-^1) \,. \tag{6.5}$$

The distribution in eq. (6.1) can be written as the sum of ten angular terms, four corresponding to the square of the transversity amplitude of each final state polarisation, and six corresponding to the cross terms describing interference among the final polarisations.

The modulus of a given transversity amplitude, A_x, is written as $|A_x|$, and its phase as δ_x. The convention $\delta_0 = 0$ is used in this paper. The P-wave polarisation fractions are $f_i = |A_i|^2/(|A_0|^2 + |A_\parallel|^2 + |A_\perp|^2)$, with $i = 0, \parallel, \perp$ and the S-wave fraction is defined as $F_{\text{S}} = |A_{\text{S}}|^2/(|A_0|^2 + |A_\parallel|^2 + |A_\perp|^2 + |A_{\text{S}}|^2)$. The distribution of the CP-conjugate decay is obtained by flipping the sign of the interference terms which contain $|A_\perp|$. For the CP-conjugate case, the amplitudes are denoted as $\overline{A}_i$. Each A_i and the corresponding $\overline{A}_i$ are related through the CP asymmetries, as described in section 6.3.

6.2 Partial-wave interference factors

In the general case, the transversity amplitudes of the angular model depend on the $K^-\pi^+$ mass ($m_{K^-\pi^+}$). This variable is limited to be inside a window of $\pm 70\,\text{MeV}/c^2$ around the $\overline{K}^{*0}$ mass. Figure 4 shows the efficiency-corrected $m_{K^-\pi^+}$ spectra for B_s^0 and B^0 using the nominal sets of *sWeights*.

In order to account for the $m_{K^-\pi^+}$ dependence while keeping the framework of an angular-only analysis, a fit is performed simultaneously in the same four $m_{K^-\pi^+}$ bins defined in section 5. Different values of the parameters $|A_{\text{S}}|^2$ and δ_{S} are allowed for each bin, but the angular distribution still contains mass-dependent terms associated with the interference between partial-waves. If only the S-wave and P-wave are considered, such interference terms correspond to the following complex integrals,

$$\frac{\int_{m_{K\pi}^L}^{m_{K\pi}^H} \mathcal{P} \times \mathcal{S}^* \, \Phi \, \varepsilon_m(m_{K\pi}) \, \mathrm{d}m_{K\pi}}{\sqrt{\int_{m_{K\pi}^L}^{m_{K\pi}^H} |\mathcal{P}|^2 \, \Phi \, \varepsilon_m(m_{K\pi}) \, \mathrm{d}m_{K\pi} \int_{m_{K\pi}^L}^{m_{K\pi}^H} |\mathcal{S}|^2 \, \Phi \, \varepsilon_m(m_{K\pi}) \, \mathrm{d}m_{K\pi}}} = C_{\text{SP}} e^{-\mathrm{i}\theta_{\text{SP}}} \,, \tag{6.6}$$

where $m_{K\pi}^{L(H)}$ is the lower (higher) limit of the bin, $\varepsilon_m(m_{K\pi})$ is the acceptance for a $K^-\pi^+$ candidate with mass $m_{K\pi}$ (see appendix A for a discussion on the angular acceptance), Φ stands for the phase space, and $\mathcal{P}$ ($\mathcal{S}$) is the P-wave (S-wave) propagator. The phase space term is computed as
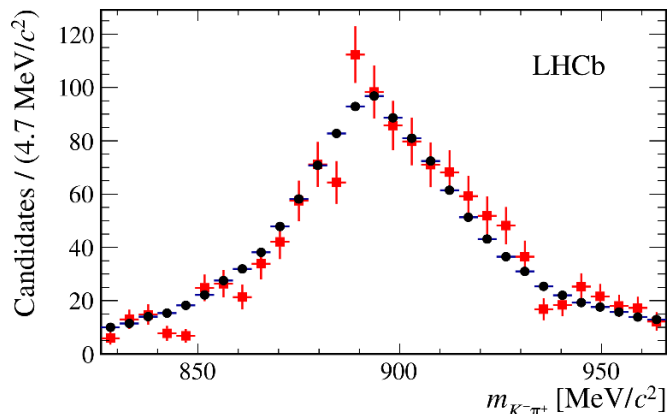
$$\Phi = \frac{p \, q}{m_{K\pi}^2} \,, \tag{6.7}$$

– 8 –

Figure 4. Efficiency corrected $m_{K^-\pi^+}$ distribution for B_s^0 shown in squares (red) and $\overline{B}^0$ shown in circles (black) using *sWeights* computed from the maximum likelihood fit to the $J/\psi K^-\pi^+$ invariant mass spectrum.

Bin	$m_{K^-\pi^+}$ range (MeV/c^2)	$C_{\rm SP}$	$C_{\rm SD}$	$C_{\rm PD}$
0	$[826, 861]$	0.968 ± 0.017	0.9968 ± 0.0030	0.9827 ± 0.0048
1	$[861, 896]$	0.931 ± 0.012	0.9978 ± 0.0021	0.9402 ± 0.0048
2	$[896, 931]$	0.952 ± 0.012	0.9983 ± 0.0016	0.9421 ± 0.0056
3	$[931, 966]$	0.988 ± 0.011	0.9986 ± 0.0012	0.9802 ± 0.0066

Table 2. The $C_{\rm SP}$, $C_{\rm SD}$ and $C_{\rm PD}$ factors calculated in each of the four $m_{K^-\pi^+}$ bins around the $\overline{K}^{*0}$ peak.

where p denotes the $\overline{K}^{*0}$ momentum in the B_s^0 rest frame and q refers to the K^- momentum in the $\overline{K}^{*0}$ rest frame.

The phase $\theta_{\rm SP}$ is included in the definition of $\delta_{\rm S}$ but the $C_{\rm SP}$ factors, corresponding to real numbers in the interval $[0, 1]$, have to be computed and input to the angular fit. The contribution of D-wave ($J = 2$) in the $m_{K^-\pi^+}$ range considered is expected to be negligible. Therefore the nominal model only includes S-wave and P-wave. To determine the systematic uncertainty due to possible D-wave contributions, $C_{\rm SD}$ and $C_{\rm PD}$ factors are also computed, using analogous expressions to that given in eq. (6.6). The C_{ij} factors are calculated by evaluating numerically the integrals using the propagators outlined below, and are included as fixed parameters in the fit. A systematic uncertainty associated to the different possible choices of the propagator models is afterwards evaluated.

The S-wave propagator is constructed using the LASS parametrisation [39], consisting of a linear combination of the $K_0^*(1430)^0$ resonance with a non-resonant term, coming from elastic scattering. The P-wave is described by a combination of the $K^*(892)^0$ and $K_1^*(1410)^0$ resonances using the isobar model [40], and the D-wave is assumed to come from the $K_2^*(1430)^0$ contribution. Relativistic Breit-Wigner functions, multiplied by angular momentum barrier factors, are used to parametrise the different resonances. Table 2 contains the computed $C_{\rm SP}$, $C_{\rm SD}$ and $C_{\rm PD}$ factors.

6.3 CP asymmetries

The direct CP violation asymmetry in the $B_{(s)}^0$ decay rate to the final state $f_{(s)\,i}$, with $f_{s,i} = J/\psi\,(K^-\pi^+)_i$ and $f_i = J/\psi\,(K^+\pi^-)_i$, is defined as

$$A_i^{CP}(B_{(s)}^0 \to f_{(s)\,i}) = \frac{|\overline{A}_{(s)\,i}|^2 - |A_{(s)\,i}|^2}{|\overline{A}_{(s)\,i}|^2 + |A_{(s)\,i}|^2}\,, \tag{6.8}$$

where $A_{(s)\,i}$ are the transversity amplitudes defined in section 6.1 and the additional index s is used to distinguish the B_s^0 and the B^0-meson. The index i refers to the polarisation of the final state ($i = 0, \|, \perp, \mathrm{S}$) and is dropped in the rest of this section, for clarity.

The raw CP asymmetry is expressed in terms of the number of observed candidates by

$$A_{\mathrm{raw}}^{CP}(B_{(s)}^0 \to f_{(s)}) = \frac{N^{\mathrm{obs}}(\overline{f}_{(s)}) - N^{\mathrm{obs}}(f_{(s)})}{N^{\mathrm{obs}}(\overline{f}_{(s)}) + N^{\mathrm{obs}}(f_{(s)})}\,. \tag{6.9}$$

Both asymmetries in eq. (6.8) and eq. (6.9) are related by [41]

$$A^{CP}(B_{(s)}^0 \to f_{(s)}) \simeq A_{\mathrm{raw}}^{CP}(B_{(s)}^0 \to f_{(s)}) - \zeta_{(s)} A_{\mathrm{D}}(f) - \kappa_{(s)} A_{\mathrm{P}}(B_{(s)}^0)\,, \tag{6.10}$$

where $A_{\mathrm{D}}(f)$ is the detection asymmetry, defined as in eq. (6.13), $A_{\mathrm{P}}(B_{(s)}^0)$ is the $B_{(s)}^0 - \overline{B}_{(s)}^0$ production asymmetry, defined as in eq. (6.12), $\zeta_{(s)} = +1(-1)$ and $\kappa_{(s)}$ accounts for the dilution due to $B_{(s)}^0 - \overline{B}_{(s)}^0$ oscillations [42]. The $\kappa_{(s)}$ factor is evaluated by

$$\kappa_{(s)} = \frac{\int_0^\infty e^{-\Gamma_{(s)}t} \cos(\Delta m_{(s)} t)\varepsilon(t)\mathrm{d}t}{\int_0^\infty e^{-\Gamma_{(s)}t} \cosh\left(\frac{\Delta\Gamma_{(s)}}{2}t\right)\varepsilon(t)\mathrm{d}t}\,, \tag{6.11}$$

where $\varepsilon(t)$ is the time-dependent acceptance function, assumed to be identical for the $B_s^0 \to J/\psi\,\overline{K}^{*0}$ and $B^0 \to J/\psi\,K^{*0}$ decays. The symbols $\Gamma_{(s)}$ and $\Delta m_{(s)}$ denote the decay width and mass differences between the $B_{(s)}^0$ mass eigenstates.

The $B_{(s)}^0 - \overline{B}_{(s)}^0$ production asymmetry is defined as

$$A_{\mathrm{P}}\left(B_{(s)}^0\right) \equiv \frac{\sigma\left(\overline{B}_{(s)}^0\right) - \sigma\left(B_{(s)}^0\right)}{\sigma\left(\overline{B}_{(s)}^0\right) + \sigma\left(B_{(s)}^0\right)}\,, \tag{6.12}$$

where σ is the $B_{(s)}^0$ production cross-section within the LHCb acceptance. The production asymmetries reported in ref. [43] are reweighted in bins of $B_{(s)}^0$ transverse momentum to obtain

$$A_{\mathrm{P}}(B^0) = (-1.04 \pm 0.48\,(\mathrm{stat}) \pm 0.14\,(\mathrm{syst}))\,\%\,,$$
$$A_{\mathrm{P}}(B_s^0) = (-1.64 \pm 2.28\,(\mathrm{stat}) \pm 0.55\,(\mathrm{syst}))\,\%\,.$$

The $\kappa_{(s)}$ factor in eq. (6.11) is determined by fixing $\Delta\Gamma_{(s)}$, $\Delta m_{(s)}$ and $\Gamma_{(s)}$ to their world average values [30] and by fitting the decay time acceptance $\varepsilon(t)$ to the nominal data sample after applying the B^0 *sWeights*, in a similar way to ref. [44]. It is equal to 0.06% for B_s^0

decays, and 41% for B^0. This reduces the effect of the production asymmetries to the level of 10^{-5} for $B_s^0 \to J/\psi\,\overline{K}^{*0}$ and 10^{-3} for $B^0 \to J/\psi\,K^{*0}$ decays.

Other sources of asymmetries arise from the different final-state particle interactions with the detector, event reconstruction and detector acceptance. The detection asymmetry, $A_{\mathrm{D}}(f)$, is defined in terms of the detection efficiencies of the final states, $\varepsilon^{\mathrm{det}}$, as

$$A_{\mathrm{D}}(f) \equiv \frac{\varepsilon^{\mathrm{det}}(\overline{f}) - \varepsilon^{\mathrm{det}}(f)}{\varepsilon^{\mathrm{det}}(\overline{f}) + \varepsilon^{\mathrm{det}}(f)}. \tag{6.13}$$

The detection asymmetry, measured in bins of the K^+ momentum in ref. [45], is weighted with the momentum distribution of the kaon from the $B_{(s)}^0 \to J/\psi\,K^{*0}(\overline{K}^{*0})$ decays to give

$$A_{\mathrm{D}}(B^0) = (1.12 \pm 0.55\,(\mathrm{stat}))\,\%\,,$$
$$A_{\mathrm{D}}(B_s^0) = (-1.09 \pm 0.53\,(\mathrm{stat}))\,\%\,.$$

7 Measurement of $\mathcal{B}(B_s^0 \to J/\psi\,\overline{K}^{*0})$

The branching fraction $\mathcal{B}(B_s^0 \to J/\psi\,\overline{K}^{*0})$ is obtained by normalising to two different channels, $B_s^0 \to J/\psi\,\phi$ and $B^0 \to J/\psi\,K^{*0}$, and then averaging the results. The expression

$$\frac{\mathcal{B}(B_s^0 \to J/\psi\,\overline{K}^{*0}) \times \mathcal{B}(K^{*0} \to K^+\pi^-)}{\mathcal{B}(B_q \to J/\psi\,X) \times \mathcal{B}(X \to h^+h^-)} = \frac{N_{B_s^0 \to J/\psi\,\overline{K}^{*0}}}{N_{B_q \to J/\psi\,X}} \times \frac{\varepsilon_{B_q \to J/\psi\,X}}{\varepsilon_{B_s^0 \to J/\psi\,\overline{K}^{*0}}} \times \frac{f_q}{f_s}, \tag{7.1}$$

is used for the normalisation to a given $B_q \to J/\psi\,X$ decay, where N refers to the yield of the given decay, ε corresponds to the total (reconstruction, trigger and selection) efficiency, and $f_q = f_s(f_d)$ are the $B_s^0(B^0)$-meson hadronisation fractions.

The event selection of $B_s^0 \to J/\psi\,\phi$ candidates consists of the same requirements as those for $B_s^0 \to J/\psi\,\overline{K}^{*0}$ candidates (see section 3), with the exception that ϕ candidates are reconstructed in the K^+K^- state so there are no pions among the final state particles. In addition to the other requirements, reconstructed ϕ candidates are required to have mass in the range $1000 < m_{K^-K^+} < 1040\,\mathrm{MeV}/c^2$ and to have a transverse momentum in excess of $1\,\mathrm{GeV}/c^2$.

7.1 Efficiencies obtained in simulation

A first estimate of the efficiency ratios is taken from simulated events, where the particle identification variables are calibrated using $D^{*\pm}$ decays. The efficiency ratios estimated from simulation, for 2011 (2012) data, are $\varepsilon^{\mathrm{MC}}_{B^0 \to J/\psi\,K^{*0}}/\varepsilon^{\mathrm{MC}}_{B_s^0 \to J/\psi\,\overline{K}^{*0}} = 0.929 \pm 0.012$ (0.927 ± 0.012) and $\varepsilon^{\mathrm{MC}}_{B_s^0 \to J/\psi\,\phi}/\varepsilon^{\mathrm{MC}}_{B_s^0 \to J/\psi\,\overline{K}^{*0}} = 1.991 \pm 0.025$ (1.986 ± 0.027).

7.2 Correction factors for yields and efficiencies

The signal and normalisation channel yields obtained from a mass fit are affected by the presence of a non-resonant S-wave background as well as interference between S-wave and P-wave components. Such interference would integrate to zero for a flat angular acceptance, but not for experimental data that are subject to an angle-dependent acceptance. In

addition, the efficiencies determined in simulation correspond to events generated with an angular distribution different from that in data; therefore the angular integrated efficiency also needs to be modified with respect to simulation estimates. These effects are taken into account using a correction factor ω, which is the product of the correction factor to the angular-integrated efficiency and the correction factor to the P-wave yield:

$$\frac{N_{B_s^0 \to J/\psi \overline{K}^{*0}}}{N_{B_q \to J/\psi X}} \times \frac{\varepsilon_{B_q \to J/\psi X}}{\varepsilon_{B_s^0 \to J/\psi \overline{K}^{*0}}} = \frac{N_{B_s^0 \to J/\psi \overline{K}^{*0}}}{N_{B_q \to J/\psi X}} \times \frac{\varepsilon^{\mathrm{MC}}_{B_q \to J/\psi X}}{\varepsilon^{\mathrm{MC}}_{B_s^0 \to J/\psi \overline{K}^{*0}}} \times \frac{\omega_{B_q \to J/\psi X}}{\omega_{B_s^0 \to J/\psi \overline{K}^{*0}}}, \qquad (7.2)$$

where $N_{B_s^0 \to J/\psi \overline{K}^{*0}}$, $N_{B_q \to J/\psi X}$ are the yields obtained from the mass fits, $\varepsilon^{\mathrm{MC}}_{B_q \to J/\psi X}$, $\varepsilon^{\mathrm{MC}}_{B_s^0 \to J/\psi \overline{K}^{*0}}$ are the efficiencies obtained in simulation, and ω is calculated as

$$\omega_{B_q \to J/\psi X} = \frac{F^X_{B_q \to J/\psi X}}{c_{B_q \to J/\psi X}}, \qquad (7.3)$$

where $F^X_{B_q \to J/\psi X}$ is the fraction of the P-wave X resonance in a given $B_q \to J/\psi X$ decay (related to the presence of S-wave and its interference with the P-wave), and $c_{B_q \to J/\psi X}$ is a correction to $\varepsilon^{\mathrm{MC}}_{B_q \to J/\psi X}$ due to the fact that the simulated values of the decay parameters differ slightly from those measured. The values obtained for the ω correction factors are

$$\omega_{B_s^0 \to J/\psi \overline{K}^{*0}} = 1.149 \pm 0.044\,(\mathrm{stat}) \pm 0.018\,(\mathrm{syst})\,,$$
$$\omega_{B^0 \to J/\psi K^{*0}} = 1.107 \pm 0.003\,(\mathrm{stat}) \pm 0.038\,(\mathrm{syst})\,,$$
$$\omega_{B_s^0 \to J/\psi \phi} = 1.013 \pm 0.002\,(\mathrm{stat}) \pm 0.007\,(\mathrm{syst})\,.$$

7.3 Normalisation to $B_s^0 \to J/\psi \phi$

The study of penguin pollution requires the calculation of ratios of absolute amplitudes between $B_s^0 \to J/\psi \overline{K}^{*0}$ and $B_s^0 \to J/\psi \phi$. Thus, normalising $\mathcal{B}(B_s^0 \to J/\psi \overline{K}^{*0})$ to $\mathcal{B}(B_s^0 \to J/\psi \phi)$ is very useful. This normalisation is given by

$$\frac{\mathcal{B}(B_s^0 \to J/\psi \overline{K}^{*0})}{\mathcal{B}(B_s^0 \to J/\psi \phi)} = \frac{N_{B_s^0 \to J/\psi K^- \pi^+}}{N_{B_s^0 \to J/\psi K^+ K^-}} \times \frac{\varepsilon^{\mathrm{MC}}_{B_s^0 \to J/\psi \phi}}{\varepsilon^{\mathrm{MC}}_{B_s^0 \to J/\psi \overline{K}^{*0}}} \times \frac{\omega_{B_s^0 \to J/\psi \phi}}{\omega_{B_s^0 \to J/\psi \overline{K}^{*0}}} \times \frac{\mathcal{B}(\phi \to K^+ K^-)}{\mathcal{B}(\overline{K}^{*0} \to K^- \pi^+)}, \qquad (7.4)$$

where $\mathcal{B}(\overline{K}^{*0} \to K^- \pi^+) = 2/3$ and $\mathcal{B}(\phi \to K^+ K^-) = (49.5 \pm 0.5)\%$ [30]. Using $N_{B_s^0 \to J/\psi K^- \pi^+}$ as given in eq. (5.3), and $N_{B_s^0 \to J/\psi K^+ K^-} = 58\,091 \pm 243\,(\mathrm{stat}) \pm 319\,(\mathrm{syst})$ as obtained from a fit to the invariant mass of selected $B_s^0 \to J/\psi \phi$ candidates, where the signal is described by a double-sided Hypatia distribution and the combinatorial background is described by an exponential distribution, a value of

$$\frac{\mathcal{B}(B_s^0 \to J/\psi \overline{K}^{*0})}{\mathcal{B}(B_s^0 \to J/\psi \phi)} = \big(4.05 \pm 0.19(\mathrm{stat}) \pm 0.13(\mathrm{syst})\big)\%$$

is obtained.

7.4 Normalisation to $B^0 \to J/\psi K^{*0}$

The normalisation to $B^0 \to J/\psi K^{*0}$ is given by

$$\frac{\mathcal{B}(B_s^0 \to J/\psi \overline{K}^{*0})}{\mathcal{B}(B^0 \to J/\psi K^{*0})} = \frac{N_{B_s^0 \to J/\psi K^- \pi^+}}{N_{B^0 \to J/\psi K^+ \pi^-}} \times \frac{f_d}{f_s} \times \frac{\varepsilon_{B^0 \to J/\psi K^{*0}}^{\mathrm{MC}}}{\varepsilon_{B_s^0 \to J/\psi \overline{K}^{*0}}^{\mathrm{MC}}} \times \frac{\omega_{B^0 \to J/\psi K^{*0}}}{\omega_{B_s^0 \to J/\psi \overline{K}^{*0}}} \,, \qquad (7.5)$$

where $N_{B^0 \to J/\psi K^+ \pi^-}$ and $N_{B_s^0 \to J/\psi K^- \pi^+}$ are given in eq. (5.2) and eq. (5.3), respectively, and

$$\frac{\omega_{B^0 \to J/\psi K^{*0}}}{\omega_{B_s^0 \to J/\psi \overline{K}^{*0}}} = 0.963 \pm 0.036 \,(\mathrm{stat}) \pm 0.031 \,(\mathrm{syst}) \,,$$

resulting in a value of

$$\frac{\mathcal{B}(B_s^0 \to J/\psi \overline{K}^{*0})}{\mathcal{B}(B^0 \to J/\psi K^{*0})} = (2.99 \pm 0.14 \,(\mathrm{stat}) \pm 0.12 \,(\mathrm{syst}) \pm 0.17 \,(f_d/f_s)) \,\% \,, \qquad (7.6)$$

where the third uncertainty comes from the hadronisation fraction ratio $f_d/f_s = 3.86 \pm 0.22$ [7].

7.5 Computation of $\mathcal{B}(B_s^0 \to J/\psi \overline{K}^{*0})$

By multiplying the fraction given in eq. (7.6) by the branching fraction of the decay $B^0 \to J/\psi K^{*0}$ measured at Belle,[2] $(1.29 \pm 0.05 \,(\mathrm{stat}) \pm 0.13 \,(\mathrm{syst})) \times 10^{-3}$ [46], and taking into account the difference in production rates for the $B^+ B^-$ and $B^0 \overline{B}^0$ pairs at the $\Upsilon(4S)$ resonance, i.e. $\Gamma(B^+ B^-)/\Gamma(B^0 \overline{B}^0) = 1.058 \pm 0.024$ [7], the value

$$\mathcal{B}(B_s^0 \to J/\psi \overline{K}^{*0})_d = (3.95 \pm 0.18 \,(\mathrm{stat}) \pm 0.16 \,(\mathrm{syst}) \pm 0.23 \,(f_d/f_s)$$
$$\pm 0.43 \,(\mathcal{B}(B^0 \to J/\psi K^{*0}))) \times 10^{-5}$$

is obtained, where the fourth uncertainty arises from $\mathcal{B}(B^0 \to J/\psi K^{*0})$. A second estimate of this quantity is found via the normalisation to $\mathcal{B}(B_s^0 \to J/\psi \phi)$ [32], updated with the value of f_d/f_s from ref. [7] to give $\mathcal{B}(B_s^0 \to J/\psi \phi) = (1.038 \pm 0.013 \,(\mathrm{stat}) \pm 0.063 \,(\mathrm{syst}) \pm 0.060 \,(f_d/f_s)) \times 10^{-3}$, resulting in a value of

$$\mathcal{B}(B_s^0 \to J/\psi \overline{K}^{*0})_\phi = \left(4.20 \pm 0.20 \,(\mathrm{stat}) \pm 0.13 \,(\mathrm{syst}) \pm 0.36 \,(\mathcal{B}(B_s^0 \to J/\psi \phi))\right) \times 10^{-5} \,,$$

where the third uncertainty comes from $\mathcal{B}(B_s^0 \to J/\psi \phi)$. Both values are compatible within uncorrelated systematic uncertainties and are combined, taking account of correlations, to give

$$\mathcal{B}(B_s^0 \to J/\psi \overline{K}^{*0}) = (4.14 \pm 0.18 \,(\mathrm{stat}) \pm 0.26 \,(\mathrm{syst}) \pm 0.24 \,(f_d/f_s)) \times 10^{-5} \,,$$

which is in good agreement with the previous LHCb measurement [16], of $(4.4^{+0.5}_{-0.4} \pm 0.8) \times 10^{-5}$.

---

[2] The result from Belle was chosen rather than the PDG average, since it is the only $\mathcal{B}(B^0 \to J/\psi K^{*0})$ measurement that subtracts S-wave contributions.
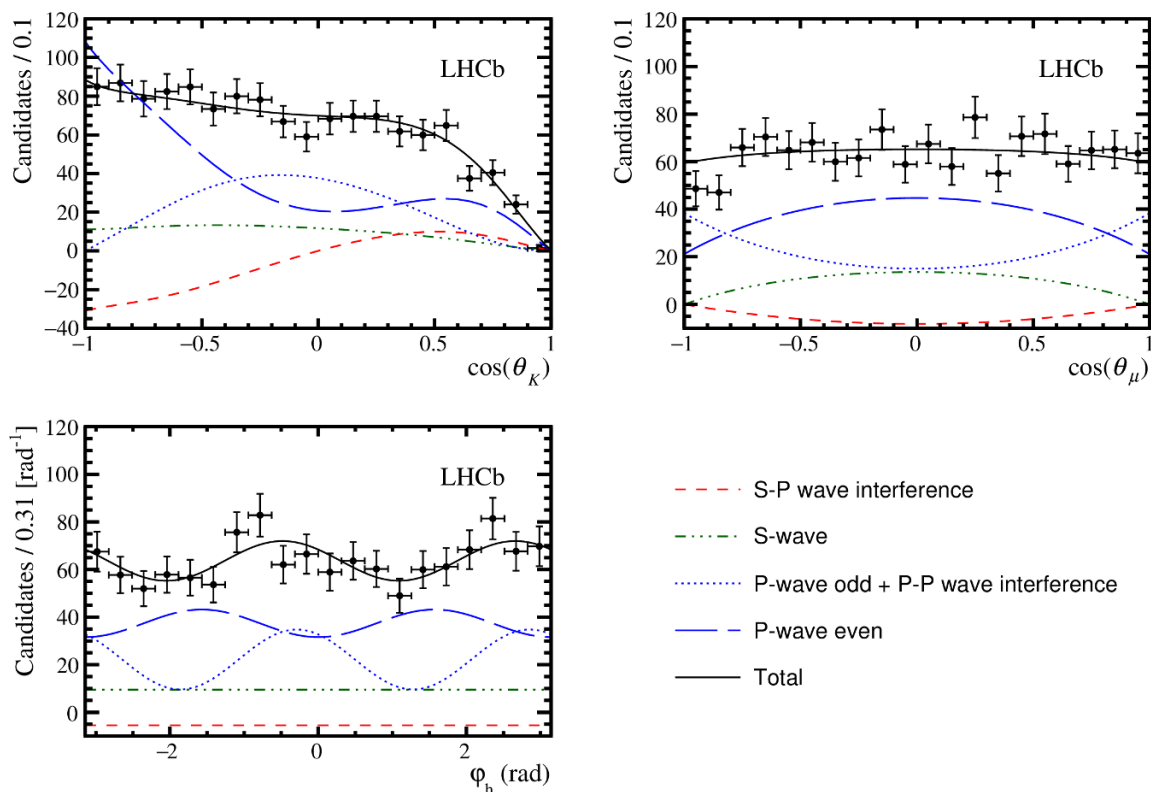
Figure 5. Fitted signal distributions compared with the weighted angular distributions with B_s^0 *sWeights*. Points with error bars show the data. The projection of the fit result is represented by the solid black line, and the contributions from the different amplitude components are described in the legend.

8 Results and systematic uncertainties

Section 8.1 presents the results of the angular fit as well as the procedure used to estimate the systematic uncertainties, while in section 8.2 the results of the branching fraction measurements and the corresponding estimated systematic uncertainties are discussed.

8.1 Angular parameters and *CP* asymmetries

The results obtained from the angular fit to the $B_s^0 \to J/\psi \, \overline{K}^{*0}$ events are given in table 3 and table 4 for the P-wave and S-wave parameters, respectively. For comparison, the previous LHCb measurements [16] of f_0 and $f_\parallel$ were $0.50 \pm 0.08 \pm 0.02$ and $0.19^{+0.10}_{-0.08} \pm 0.02$, respectively. The angular distribution of the signal and the projection of the fitted distribution are shown in figure 5. The statistical-only correlation matrix as obtained from the fit to data is given in appendix B. The polarisation-dependent *CP* asymmetries are compatible with zero, as expected in the SM. The polarisation fractions are in good agreement with the previous measurements [16] performed on the same decay mode by the LHCb collaboration using data corresponding to an integrated luminosity of $0.37\,\mathrm{fb}^{-1}$.

Various sources of systematic uncertainties on the parameters of the angular fit are studied, as summarised in table 3 and table 4 for the P-wave and S-wave parameters. Two

classes of systematic uncertainties are defined, one from the angular fit model and another from the mass fit model. Since the angular fit is performed on the data weighted using the signal *sWeights* calculated from the fit to the $J/\psi K^- \pi^+$ invariant mass, biases on the mass fit results may be propagated to the *sWeights* and thus to the angular parameters. Overall, two sources of systematic uncertainties dominate: the angular acceptance and the correlation between the $J/\psi K^- \pi^+$ invariant mass and θ_μ.

8.1.1 Systematic uncertainties related to the mass fit model

To determine the systematic uncertainty arising from the fixed parameters in the description of the $J/\psi K^- \pi^+$ invariant mass, these parameters are varied inside their uncertainties, as determined from fits to simulated events. The fit is then repeated and the widths of the B_s^0 and B^0 yield distributions are taken as systematic uncertainties on the branching fractions. Correlations among the parameters obtained from simulation are taken into account in this procedure. For each new fit to the $J/\psi K^- \pi^+$ invariant mass, the corresponding set of *sWeights* is calculated and the fit to the weighted angular distributions is repeated. The widths of the distributions are taken as systematic uncertainties on the angular parameters. In addition, a systematic uncertainty is added to account for imperfections in the modelling of the upper tail of the B^0 and B_s^0 peaks. Indeed, in the Hypatia distribution model, the parameters a_2 and n_2 take into account effects such as decays in flight of the hadron, that affect the lineshape of the upper tail and could modify the B^0 leakage into the B_s^0 peak. The estimate of this leakage is recalculated for extreme values of those parameters, and the maximum spread is conservatively added as a systematic uncertainty.

Systematic uncertainties due to the fixed yields of the $B_s^0 \to J/\psi K^+ K^-$, $B_s^0 \to J/\psi \pi^+ \pi^-$, $B^0 \to J/\psi \pi^+ \pi^-$, and $\Lambda_b^0 \to J/\psi p K^-$ peaking backgrounds,[3] are evaluated by repeating the fit to the invariant mass varying the normalisation of all background sources by either plus or minus one standard deviation of its estimated yield. For each of the new mass fits, the angular fit is repeated using the corresponding new sets of *sWeights*. The deviations on each of the angular parameters are then added in quadrature.

Correlations between the $J/\psi K^- \pi^+$ invariant mass and the cosine of the helicity angle θ_μ are taken into account in the nominal fit model, where the mass fit is performed in five bins of $\cos(\theta_\mu)$. In order to evaluate systematic uncertainties due to these correlations, the mass fit is repeated with the full range of $\cos(\theta_\mu)$ divided into four or six equal bins. For each new mass fit, the angular fit is repeated using the corresponding set of *sWeights*. The deviations from the nominal result for each of the variations are summed quadratically and taken as the systematic uncertainty.

8.1.2 Systematic uncertainties related to the angular fit model

In order to account for systematic uncertainties due to the angular acceptance, two distinct effects are considered, as in ref. [8]. The first is due to the limited size of the simulation sample used in the acceptance estimation. It is estimated by varying the normalisation

---

[3]The yields of the subtracted backgrounds can be considered as fixed, since the sum of negative weights used to subtract them is constant in the nominal fit.

	f_0	$f_\parallel$	$\delta_\parallel$	$\delta_\perp$	A_0^{CP}	$A_\parallel^{CP}$	$A_\perp^{CP}$
Fitted value	0.497	0.179	-2.70	0.01	-0.048	0.171	-0.049
Statistical uncertainties	0.025	0.027	0.16	0.11	0.057	0.152	0.096
Angular acceptance (simulation statistics)	0.018	0.008	0.02	0.01	0.009	0.017	0.008
Angular acceptance (data-simulation differences)	0.015	0.007	0.17	0.10	0.007	—	0.015
$C_{\rm SP}$ factors	—	0.001	—	—	0.001	0.002	0.002
D-wave contribution	0.004	0.003	—	—	0.002	0.015	0.002
Background angular model	0.004	0.002	0.02	0.01	0.004	$+0.012$ -0.004	0.002
Mass parameters and B^0 contamination	—	—	—	—	0.001	0.001	—
Mass–$\cos(\theta_\mu)$ correlations	0.007	0.006	0.07	$+0.02$ -0.04	0.014	$+0.009$ -0.012	0.016
Fit bias	—	0.001	0.01	0.07	0.003	0.002	0.005
Detection asymmetry	—	—	—	—	0.005	0.005	0.006
Production asymmetry	—	—	—	—	—	—	—
Quadratic sum of systematic uncertainties	0.025	0.013	0.19	$+0.012$ -0.013	0.020	$+0.028$ -0.027	0.025
Total uncertainties	0.035	0.030	0.25	$+0.016$ -0.017	0.060	0.154	0.099

Table 3. Summary of the measured $B_s^0 \to J/\psi \overline{K}^{*0}$ P-wave properties and their statistical and systematic uncertainties. When no value is given, it means an uncertainty below 5×10^{-4}, except for the two phases, $\delta_\parallel$ (rad) and $\delta_\perp$ (rad), in which case the uncertainty is below 5×10^{-3}.

weights 200 times following a Gaussian distribution within a five standard deviation range taking into account their correlations. For each of these sets of normalisation weights, the angular fit is repeated, resulting in a distribution for each fitted parameter. The width of the resulting parameter distribution is taken as the systematic uncertainty. Note that in this procedure, the normalisation weights are varied independently in each $m_{K^-\pi^+}$ bin. The second effect, labelled as data-simulation corrections in the tables, accounts

| | $A_{\rm S}^{CP}$ | $m_{K^-\pi^+}^{\rm bin0}$ | | $m_{K^-\pi^+}^{\rm bin1}$ | | $m_{K^-\pi^+}^{\rm bin2}$ | | $m_{K^-\pi^+}^{\rm bin3}$ | |
		$F_{\rm S}$	$\delta_{\rm S}$	$F_{\rm S}$	$\delta_{\rm S}$	$F_{\rm S}$	$\delta_{\rm S}$	$F_{\rm S}$	$\delta_{\rm S}$
Fitted value	0.167	0.475	0.54	0.080	-0.53	0.044	-1.46	0.523	-1.76
Statistical uncertainties	0.114	$+0.108$ -0.112	0.16	$+0.031$ -0.025	$+0.25$ -0.21	$+0.042$ -0.029	$+0.22$ -0.19	$+0.109$ -0.112	$+0.13$ -0.14
Angular acceptance (simulation statistics)	0.028	0.039	0.03	0.012	0.065	0.015	0.10	0.065	0.06
Angular acceptance (data-simulation differences)	0.015	0.058	0.08	0.019	0.18	0.027	0.27	0.006	0.04
$C_{\rm SP}$ factors	—	0.002	0.01	0.001	—	0.002	—	0.001	0.01
D-wave contribution	0.008	0.010	0.02	0.005	0.03	0.008	0.08	0.002	0.04
Background angular model	0.001	0.002	0.01	$+0.000$ -0.001	0.01	—	0.03	$+0.002$ -0.000	$+0.07$ -0.04
Mass parameters and B^0 contamination	0.001	0.001	0.01	—	—	—	—	—	—
Mass–$\cos(\theta_\mu)$ correlations	$+0.023$ -0.029	$+0.040$ -0.028	0.05	0.003	0.04	$+0.006$ -0.016	0.02	$+0.009$ -0.011	0.03
Fit bias	0.004	0.005	0.01	0.003	0.02	0.007	0.032	0.015	0.01
Detection asymmetry	0.005	—	—	—	—	—	—	—	—
Production asymmetry	—	—	—	—	—	—	—	—	—
Quadratic sum of systematic uncertainties	$+0.041$ -0.044	$+0.081$ -0.076	0.10	0.023	0.20	$+0.033$ -0.036	0.30	0.068	$+0.11$ -0.09
Total uncertainties	$+0.120$ -0.122	0.135	0.19	$+0.039$ -0.034	$+0.32$ -0.29	$+0.054$ -0.047	$+0.37$ -0.35	$+0.128$ -0.131	0.17

Table 4. Summary of the measured $B_s^0 \to J/\psi \overline{K}^{*0}$ S-wave properties and their statistical and systematic uncertainties. When no value is given, it means an uncertainty below 5×10^{-4}, except for the four phases related to the S-wave component, $\delta_{\rm S}$ (rad), in which case the uncertainty is below 5×10^{-3}. The $m_{K^-\pi^+}$ binning definition is identical to the one given in table 2.

for differences between the data and the simulation, using normalisation weights that are determined assuming the amplitudes measured in ref. [47]. The difference with respect to the nominal fit is assigned as a systematic uncertainty. The uncertainties due to the choice of model for the $C_{\rm SP}$ factors are evaluated as the maximum differences observed in the measured parameters when computing the $C_{\rm SP}$ factors with all of the alternative models, as discussed below. Instead of the nominal propagator for the S-wave, a combination of the $K_0^*(800)^0$ and $K_0^*(1430)^0$ resonances with a non-resonant term using the isobar model

is considered, as well as a K-matrix [48] version. A pure phase space term is also used, in order to account for the simplest possible parametrisation. For the P-wave, the alternative propagators considered are the $K^*(892)^0$ alone and a combination of this contribution with the $K_1^*(1410)^0$ and the $K_1^*(1430)^0$ using the isobar model.

In order to account for the absence of D-wave terms in the nominal fit model a new fit is performed, including a D-wave component, where the related parameters are fixed to the values measured in the $K_2^*(1430)^0$ region. The differences in the measured parameters between the results obtained with and without a D-wave component are taken as the corresponding systematic uncertainty.

The presence of biases in the fit model itself is studied using parametric simulation. For this study, 1000 pseudoexperiments were generated and fitted using the nominal shapes, where the generated parameter values correspond to the ones obtained in the fit to data. The difference between the generated value and the mean of the distribution of fitted parameter values are treated as a source of systematic uncertainty.

Finally, the systematic uncertainties due to the fixed values of the detection and production asymmetries are estimated by varying their values by ± 1 standard deviation and repeating the fit.

8.2 Branching fraction

Several sources of systematic uncertainties on the branching fraction measurements are studied, summarised along with the results in table 5: systematic uncertainties due to the external parameter f_d/f_s and due to the branching fraction $\mathcal{B}(\phi \to K^+K^-)$; systematic uncertainties due to the ratio of efficiencies obtained from simulation and due to the angular parameters, propagated into the ω factors (see section 8.1); and systematic uncertainties affecting the $B_s^0 \to J/\psi \overline{K}^{*0}$ and $B^0 \to J/\psi K^{*0}$ yields, which are determined from the fit to the $J/\psi K^+\pi^-$ invariant mass and described in section 8.1. Finally, a systematic uncertainty due to the $B_s^0 \to J/\psi \phi$ yield determined from the fit to the $J/\psi K^+K^-$ invariant mass distribution, described in section 7.3, is also taken into account, where only the effect due to the modelling of the upper tail of the B_s^0 peak is considered (see section 8.1.1). For the computation of the absolute branching fraction $\mathcal{B}(B_s^0 \to J/\psi \overline{K}^{*0})$ (see section 7.5), two additional systematic sources are taken into account, the uncertainties in the external parameters $\mathcal{B}(B^0 \to J/\psi K^{*0})$ and $\mathcal{B}(B_s^0 \to J/\psi \phi)$.

9 Penguin pollution in ϕ_s

9.1 Information from $B_s^0 \to J/\psi \overline{K}^{*0}$

Following the strategy proposed in refs. [9, 11, 13], the measured branching fraction, polarisation fractions and CP asymmetries can be used to quantify the contributions originating from the penguin topologies in $B_s^0 \to J/\psi \overline{K}^{*0}$. To that end, the transition amplitude for the $B_s^0 \to J/\psi \overline{K}^{*0}$ decay is written in the general form

$$A\left(B_s^0 \to (J/\psi \overline{K}^{*0})_i\right) = -\lambda \mathcal{A}_i \left[1 - a_i e^{\mathrm{i}\theta_i} e^{\mathrm{i}\gamma}\right] , \qquad (9.1)$$

Relative branching fraction	$\frac{\mathcal{B}(B_s^0 \to J/\psi \, \overline{K}^{*0})}{\mathcal{B}(B^0 \to J/\psi \, K^{*0})}$ (%)	$\frac{\mathcal{B}(B_s^0 \to J/\psi \, \overline{K}^{*0})}{\mathcal{B}(B_s^0 \to J/\psi \, \phi)}$ (%)
Nominal value	2.99	4.05
Statistical uncertainties	0.14	0.19
Efficiency ratio	0.04	0.05
Angular correction (ω)	0.09	0.07
Mass model (effect on the yield)	0.06	0.08
f_d/f_s	0.17	—
$\mathcal{B}(\phi \to K^+ K^-)$	—	0.04
Quadratic sum (excluding f_d/f_s)	0.12	0.13
Total uncertainties	0.25	0.23

Table 5. Summary of the measured values for the relative branching fractions and their statistical and systematic uncertainties.

where $\lambda = |V_{us}| = 0.22548^{+0.00068}_{-0.00034}$ [6] and i labels the different polarisation states. In the above expression, $\mathcal{A}_i$ is a *CP*-conserving hadronic matrix element that represents the tree topology, and a_i parametrises the relative contribution from the penguin topologies. The *CP*-conserving phase difference between the two terms is parametrised by θ_i, whereas their weak phase difference is given by the angle γ of the Unitarity Triangle.

Both the branching fraction and the *CP* asymmetries depend on the penguin parameters a_i and θ_i. The dependence of A_i^{CP} is given by [9]

$$A_i^{CP} = -\frac{2a_i \sin\theta_i \sin\gamma}{1 - 2a_i \cos\theta_i \cos\gamma + a_i^2} \, . \tag{9.2}$$

To use the branching fraction information an observable is constructed [9]:

$$H_i \equiv \frac{1}{\epsilon}\left|\frac{\mathcal{A}_i'}{\mathcal{A}_i}\right|^2 \frac{\Phi\left(\frac{m_{J/\psi}}{m_{B_s^0}}, \frac{m_\phi}{m_{B_s^0}}\right)}{\Phi\left(\frac{m_{J/\psi}}{m_{B_s^0}}, \frac{m_{\overline{K}^{*0}}}{m_{B_s^0}}\right)} \frac{\mathcal{B}(B_s^0 \to J/\psi \, \overline{K}^{*0})_{\text{theo}}}{\mathcal{B}(B_s^0 \to J/\psi \, \phi)_{\text{theo}}} \frac{f_i}{f_i'} \, , \tag{9.3}$$

$$= \frac{1 - 2a_i \cos\theta_i \cos\gamma + a_i^2}{1 + 2\epsilon a_i' \cos\theta_i' \cos\gamma + \epsilon^2 a_i'^2} \, ,$$

where $f_i^{(\prime)}$ represents the polarisation fraction,

$$\epsilon \equiv \frac{\lambda^2}{1 - \lambda^2} = 0.0536 \pm 0.0003 \text{ [6]} \, , \tag{9.4}$$

and $\Phi(x, y) = \sqrt{(1 - (x - y)^2)(1 - (x + y)^2)}$ is the standard two-body phase-space function. The primed quantities refer to the $B_s^0 \to J/\psi \, \phi$ channel, while the non-primed ones refer to $B_s^0 \to J/\psi \, \overline{K}^{*0}$. The penguin parameters a_i' and θ_i' are defined in analogy to a_i and

θ_i, and parametrise the transition amplitude of the $B_s^0 \to J/\psi \phi$ decay as

$$A\left(B_s^0 \to (J/\psi \phi)_i\right) = \left(1 - \frac{\lambda^2}{2}\right) \mathcal{A}_i' \left[1 + \epsilon a_i' e^{\mathrm{i}\theta_i'} e^{\mathrm{i}\gamma}\right] . \qquad (9.5)$$

Assuming SU(3) flavour symmetry, and neglecting contributions from exchange and penguin-annihilation topologies,[4] which are present in $B_s^0 \to J/\psi \phi$ but have no counterpart in $B_s^0 \to J/\psi \overline{K}^{*0}$, we can identify

$$a_i' = a_i , \qquad \theta_i' = \theta_i . \qquad (9.6)$$

The contributions from the additional decay topologies in $B_s^0 \to J/\psi \phi$ can be probed using the decay $B^0 \to J/\psi \phi$ [13]. The current upper limit on its branching fraction is $\mathcal{B}(B^0 \to J/\psi \phi) < 1.9 \times 10^{-7}$ at 90% confidence level (C.L.) [50], which implies that the size of these additional contributions is small compared to those associated with the penguin topologies.

The H_i observables are constructed in terms of the theoretical branching fractions defined at zero decay time, which differ from the measured time-integrated branching fractions [51] due to the non-zero decay-width difference $\Delta\Gamma_s$ of the B_s^0 meson system [7]. The conversion factor between the two branching fraction definitions [51] is taken to be

$$\frac{\mathcal{B}(B \to f)_{\mathrm{theo}}}{\mathcal{B}(B \to f)} = \frac{1 - y_s^2}{1 - y_s \eta_i \cos(\phi_s^{\mathrm{SM}})} , \qquad (9.7)$$

where η_i is the CP eigenvalue of the final state, and $y_s = \Delta\Gamma_s/2\Gamma_s$. Taking values for Γ_s, $\Delta\Gamma_s$ and ϕ_s^{SM} from refs. [6, 7], the conversion factor is 1.0608 ± 0.0045 (0.9392 ± 0.0045) for the CP-even (-odd) states. For the flavour-specific $B_s^0 \to J/\psi \overline{K}^{*0}$ decay $\eta_i = 0$, resulting in a conversion factor of 0.9963 ± 0.0006. The ratios of hadronic amplitudes $|\mathcal{A}_i'/\mathcal{A}_i|$ are calculated in ref. [52] following the method described in ref. [53] and using the latest results on form factors from Light Cone QCD Sum Rules (LCSR) [54]. This leads to

$$\begin{aligned} H_0 &= 0.98 \pm 0.07 \, (\mathrm{stat}) \pm 0.06 \, (\mathrm{syst}) \pm 0.26 \, (|\mathcal{A}_i'/\mathcal{A}_i|) , \\ H_\parallel &= 0.90 \pm 0.14 \, (\mathrm{stat}) \pm 0.08 \, (\mathrm{syst}) \pm 0.21 \, (|\mathcal{A}_i'/\mathcal{A}_i|) , \\ H_\perp &= 1.46 \pm 0.14 \, (\mathrm{stat}) \pm 0.11 \, (\mathrm{syst}) \pm 0.28 \, (|\mathcal{A}_i'/\mathcal{A}_i|) . \end{aligned}$$

Assuming eq. (9.6) and external input on the Unitarity Triangle angle $\gamma = \left(73.2^{+6.3}_{-7.0}\right)^\circ$ [6], the penguin parameters a_i and θ_i are obtained from a modified least-squares fit to $\{A_i^{CP}, H_i\}$ in eq. (9.2) and eq. (9.3). The information on γ is included as a Gaussian constraint in the fit. The values obtained for the penguin parameters are

$$\begin{aligned} a_0 &= 0.04^{+0.95}_{-0.04} , & \theta_0 &= \left(40^{+140}_{-220}\right)^\circ , \\ a_\parallel &= 0.32^{+0.57}_{-0.32} , & \theta_\parallel &= -\left(15^{+148}_{-14}\right)^\circ , \\ a_\perp &= 0.44^{+0.21}_{-0.27} , & \theta_\perp &= \left(175^{+11}_{-10}\right)^\circ . \end{aligned}$$

---

[4]We follow the decomposition introduced in ref. [49].

For the longitudinal polarisation state the phase θ is unconstrained. Correlations between the experimental inputs are ignored, but the effect of including them is small. The two-dimensional confidence level contours are given in figure 6. This figure also shows, as different (coloured) bands, the constraints on the penguin parameters derived from the individual observables entering the χ^2 fit. The thick inner darker line represents the contour associated with the central value of the input quantity, while the outer darker lines represent the contours associated with the one standard deviation changes. For the parallel polarisation the central value of the H observable does not lead to physical solutions in the $\theta_\parallel$–$a_\parallel$ plane, and the thick inner line is thus absent.

When decomposed into its different sources, the angle ϕ_s takes the form

$$\phi_{s,i} = -2\beta_s + \phi_s^{\text{BSM}} + \Delta\phi_{s,i}^{J/\psi\phi}(a_i', \theta_i') , \tag{9.8}$$

where $-2\beta_s$ is the SM contribution, ϕ_s^{BSM} is a possible BSM phase, and $\Delta\phi_{s,i}^{J/\psi\phi}$ is a shift introduced by the presence of penguin pollution in the decay $B_s^0 \to J/\psi\phi$. In terms of the penguin parameters a_i' and θ_i', the shift $\Delta\phi_{s,i}^{J/\psi\phi}$ is defined as

$$\tan(\Delta\phi_{s,i}^{J/\psi\phi}) = \frac{2\epsilon a_i' \cos\theta_i' \sin\gamma + \epsilon^2 a_i'^2 \sin(2\gamma)}{1 + 2\epsilon a_i' \cos\theta_i' \cos\gamma + \epsilon^2 a_i'^2 \cos(2\gamma)} . \tag{9.9}$$

Using eqs. (9.6) and (9.9), the fit results on a_i and θ_i given above constrain this phase shift, giving

$$\Delta\phi_{s,0}^{J/\psi\phi} = 0.003^{+0.084}_{-0.011} \, (\text{stat})^{+0.014}_{-0.009} \, (\text{syst})^{+0.047}_{-0.030} \, (|\mathcal{A}_i'/\mathcal{A}_i|) ,$$

$$\Delta\phi_{s,\parallel}^{J/\psi\phi} = 0.031^{+0.047}_{-0.037} \, (\text{stat})^{+0.010}_{-0.013} \, (\text{syst}) \pm 0.032 \, (|\mathcal{A}_i'/\mathcal{A}_i|) ,$$

$$\Delta\phi_{s,\perp}^{J/\psi\phi} = -0.045 \pm 0.012 \, (\text{stat}) \pm 0.008 \, (\text{syst})^{+0.017}_{-0.024} \, (|\mathcal{A}_i'/\mathcal{A}_i|) ,$$

which is in good agreement with the values measured in ref. [15], and with the predictions given in refs. [12–14].

The above results are obtained assuming SU(3) flavour symmetry and neglecting contributions from additional decay topologies. Because $a_i e^{i\theta_i}$ represents a ratio of hadronic amplitudes, the leading factorisable SU(3)-breaking effects cancel, and the relation between $a_i e^{i\theta_i}$ and $a_i' e^{i\theta_i'}$ is only affected by non-factorisable SU(3)-breaking. This can be parametrised using two SU(3)-breaking parameters ξ and δ as

$$a_i' = \xi \times a_i , \qquad \theta_i' = \theta_i + \delta . \tag{9.10}$$

The above quoted results assume $\xi = 1$ and $\delta = 0$. The dependence of the uncertainty on $\Delta\phi_{s,i}^{J/\psi\phi}$ on the uncertainty on ξ is illustrated in figure 7, while the dependence on the uncertainty on δ is negligible for the solutions obtained for $\{a_i, \theta_i\}$.

9.2 Combination with $B^0 \to J/\psi\,\rho^0$

The information on the penguin parameters obtained from $B_s^0 \to J/\psi\,\overline{K}^{*0}$ can be complemented with similar information from the SU(3)-related mode $B^0 \to J/\psi\,\rho^0$ [15]. Both
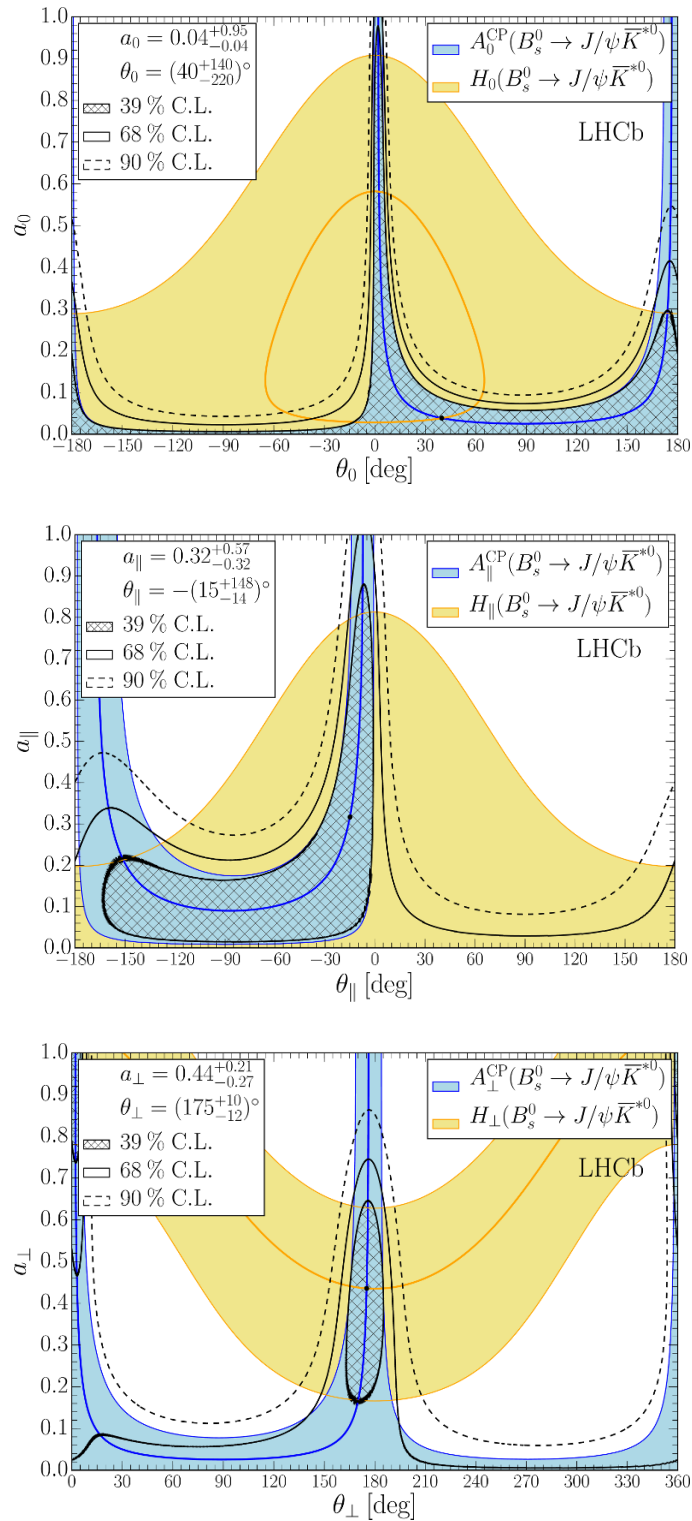
Figure 6. Limits on the penguin parameters a_i and θ_i obtained from intersecting contours derived from the *CP* asymmetries and branching fraction information in $B_s^0 \to J/\psi\,\overline{K}^{*0}$. Superimposed are the confidence level contours obtained from a χ^2 fit to the data. Shown are the longitudinal (top), parallel (middle) and perpendicular (bottom) polarisation.

Figure 7. Dependence of the uncertainty on the penguin shift $\Delta\phi_{s,i}^{J/\psi\,\phi}$ on the uncertainty on ξ. The bands correspond to the 68% C.L. The longitudinal (top), parallel (middle) and perpendicular (bottom) polarisations are shown.

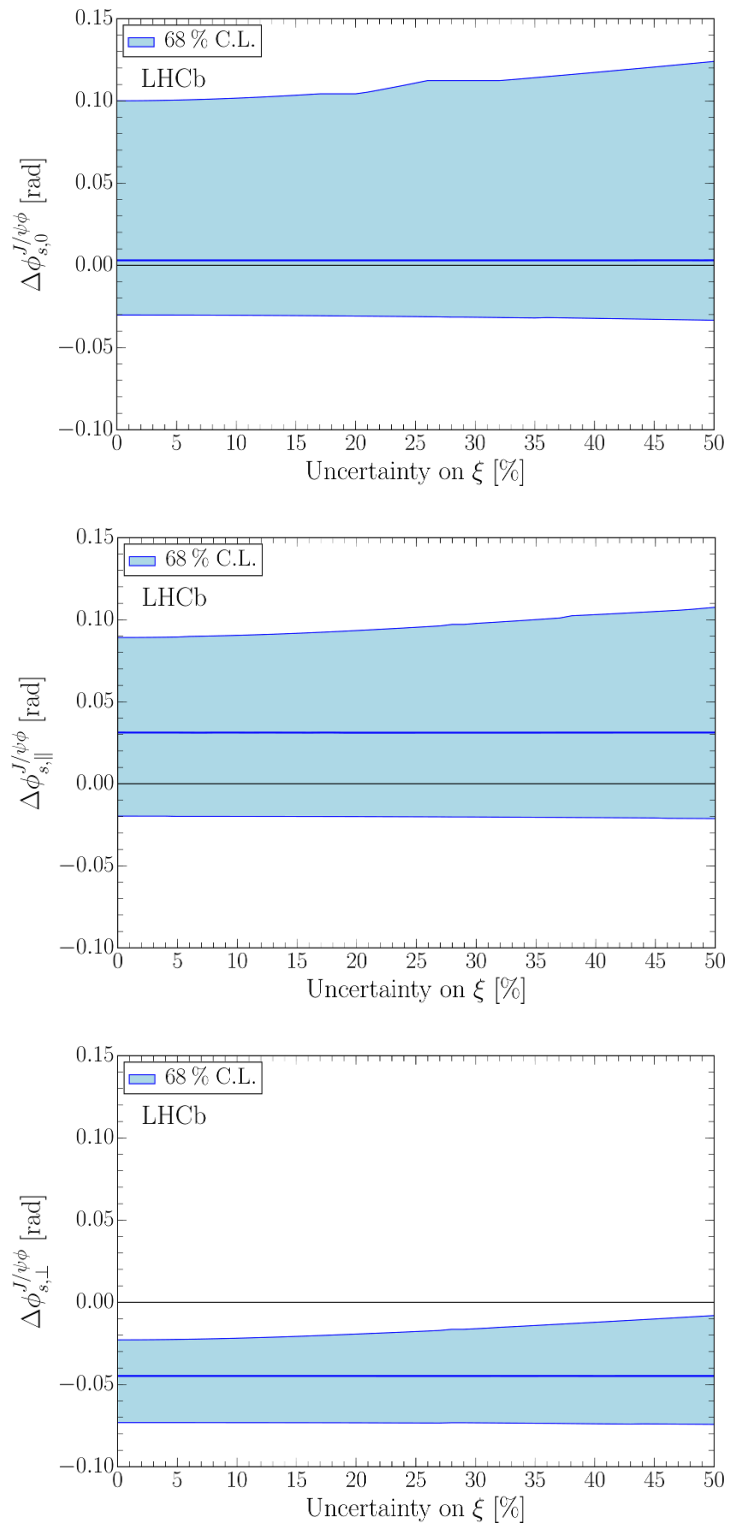modes describe a $\bar{b} \to \bar{c}c\bar{d}$ transition, and are related by exchanging the spectator $s \leftrightarrow d$ quarks. The decay amplitude of $B^0 \to J/\psi\,\rho^0$ is also parametrised as

$$A\left(B^0 \to (J/\psi\,\rho^0)_i\right) = -\lambda\tilde{\mathcal{A}}_i \left[1 - \tilde{a}_i e^{i\tilde{\theta}_i} e^{i\gamma}\right], \tag{9.11}$$

which is the equivalent of eq. (9.1). In contrast to $B_s^0 \to J/\psi\,\overline{K}^{*0}$, however, $\tilde{a}_i$ and $\tilde{\theta}_i$ also include contributions from exchange and penguin-annihilation topologies, which are present in $B^0 \to J/\psi\,\rho^0$ but have no counterpart in $B_s^0 \to J/\psi\,\overline{K}^{*0}$. Assuming SU(3) symmetry, and neglecting the contributions from the additional decay topologies in $B_s^0 \to J/\psi\,\phi$ and $B^0 \to J/\psi\,\rho^0$, the relation in eq. (9.6) can be extended to

$$a_i' = a_i = \tilde{a}_i, \qquad \theta_i' = \theta_i = \tilde{\theta}_i, \tag{9.12}$$

which allows a combined fit to be performed to the CP asymmetries and branching fraction information in $B_s^0 \to J/\psi\,\overline{K}^{*0}$ and $B^0 \to J/\psi\,\rho^0$.

The $B^0 \to J/\psi\,\rho^0$ decay exhibits decay-time-dependent CP violation, which is described by two parameters, the direct CP asymmetry C_i, which in the SU(3) limit is related to A_i^{CP} as $C_i = -A_i^{CP}$, and the mixing-induced CP asymmetry S_i. Their dependence on the penguin parameters $\tilde{a}_i$ and $\tilde{\theta}_i$ is given by

$$C_i = \frac{2\,\tilde{a}_i \sin\tilde{\theta}_i \sin\gamma}{1 - 2\,\tilde{a}_i \cos\tilde{\theta}_i \cos\gamma + \tilde{a}_i^2}, \tag{9.13}$$

$$S_i = -\eta_i \left[\frac{\sin\phi_d - 2\,\tilde{a}_i \cos\tilde{\theta}_i \sin(\phi_d + \gamma) + \tilde{a}_i^2 \sin(\phi_d + 2\gamma)}{1 - 2\,\tilde{a}_i \cos\tilde{\theta}_i \cos\gamma + \tilde{a}_i^2}\right], \tag{9.14}$$

where η_i is the polarisation-dependent CP eigenvalue of the $B^0 \to J/\psi\,\rho^0$ decay, and ϕ_d is a CP-violating phase arising from the interference between B^0–$\overline{B}^0$ mixing and the subsequent B^0 decay. The use of S_i to constrain the penguin parameters a_i and θ_i requires external information on the CP phase ϕ_d. The most precise value of ϕ_d is determined from $B^0 \to J/\psi\,K^0$ decays, but this determination is also affected by penguin pollution. A recent study of the penguin effects in $B^+ \to J/\psi\,\pi^+$, $B^+ \to J/\psi\,K^+$, $B^0 \to J/\psi\,\pi^0$ and $B^0 \to J/\psi\,K_S^0$ decays is performed in ref. [13], with the latest numerical update [52], including the results from refs. [6, 55, 56], leading to $\phi_d = 0.767 \pm 0.029\,\mathrm{rad}$.

In addition, a second set of H_i observables can be constructed by replacing $B_s^0 \to J/\psi\,\overline{K}^{*0}$ by $B^0 \to J/\psi\,\rho^0$ in eq. (9.3). To minimise the theoretical uncertainties associated with the use of these H_i observables, the strategy proposed in ref. [13] is adopted. That is, the relation

$$\left|\frac{\mathcal{A}_i'}{\mathcal{A}_i}\right| \equiv \left|\frac{\mathcal{A}_i'(B_s^0 \to J/\psi\,\phi)}{\mathcal{A}_i(B_s^0 \to J/\psi\,\overline{K}^{*0})}\right| = \left|\frac{\mathcal{A}_i'(B_s^0 \to J/\psi\,\phi)}{\mathcal{A}_i(B^0 \to J/\psi\,\rho^0)}\right| \tag{9.15}$$

between the hadronic amplitudes in $B_s^0 \to J/\psi\,\overline{K}^{*0}$ and $B^0 \to J/\psi\,\rho^0$ is assumed, and therefore relying on theoretical input from LCSR is no longer needed. Instead, the ratio $|\mathcal{A}'/\mathcal{A}|$ can be determined directly from the fit, providing experimental information on this quantity. Effectively, the three CP asymmetry parameters A_i^{CP}, C_i and S_i determine the penguin parameters a_i and θ_i. Thus, this result for a_i and θ_i predicts the values of the two

observables $H_i(B_s^0 \to J/\psi \overline{K}^{*0})$ and $H_i(B^0 \to J/\psi \rho^0)$. By comparing these two quantities with the branching fraction and polarisation information on $B_s^0 \to J/\psi \overline{K}^{*0}$, $B^0 \to J/\psi \rho^0$ and $B_s^0 \to J/\psi \phi$, the hadronic amplitude ratios $|\mathcal{A}_i'/\mathcal{A}_i|$ can be determined. The impact of the H_i observables on the penguin parameters a_i and θ_i is negligible in the combined fit.

For the combined analysis of $B_s^0 \to J/\psi \overline{K}^{*0}$ and $B^0 \to J/\psi \rho^0$ a modified least-squares fit is performed. External inputs on $\gamma = \left(73.2^{+6.3}_{-7.0}\right)^\circ$ [6] and $\phi_d = 0.767 \pm 0.029$ rad [52] are included as Gaussian constraints in the fit. The values obtained from the fit are

$$a_0 = 0.01^{+0.10}_{-0.01}, \qquad \theta_0 = -\left(83^{+97}_{-263}\right)^\circ, \qquad \left|\frac{\mathcal{A}_0'}{\mathcal{A}_0}\right| = 1.195^{+0.074}_{-0.056},$$

$$a_\| = 0.07^{+0.11}_{-0.05}, \qquad \theta_\| = -\left(85^{+72}_{-63}\right)^\circ, \qquad \left|\frac{\mathcal{A}_\|'}{\mathcal{A}_\|}\right| = 1.238^{+0.104}_{-0.080},$$

$$a_\perp = 0.04^{+0.12}_{-0.04}, \qquad \theta_\perp = \left(38^{+142}_{-218}\right)^\circ, \qquad \left|\frac{\mathcal{A}_\perp'}{\mathcal{A}_\perp}\right| = 1.042^{+0.081}_{-0.063},$$

with the two-dimensional confidence level contours given in figure 8, which also shows the constraints on the penguin parameters derived from the individual observables entering the χ^2 fit as different bands. Note that the plotted contours for the two H observables do not include the uncertainty due to $|\mathcal{A}'/\mathcal{A}|$.

The results on the penguin phase shift derived from the above results on a_i and θ_i are

$$\Delta\phi_{s,0}^{J/\psi\phi} = 0.000^{+0.009}_{-0.011}\,(\text{stat})\ ^{+0.004}_{-0.009}\,(\text{syst})\,\text{rad},$$

$$\Delta\phi_{s,\|}^{J/\psi\phi} = 0.001^{+0.010}_{-0.014}\,(\text{stat})\ \pm 0.008\,(\text{syst})\,\text{rad},$$

$$\Delta\phi_{s,\perp}^{J/\psi\phi} = 0.003^{+0.010}_{-0.014}\,(\text{stat})\ \pm 0.008\,(\text{syst})\,\text{rad}.$$

These results are dominated by the input from the CP asymmetries in $B^0 \to J/\psi \rho^0$, and show that the penguin pollution in the determination of ϕ_s is small.

10   Conclusions

Using the full LHCb Run I data sample, the branching fraction, the polarisation fractions and the direct CP violation parameters in $B_s^0 \to J/\psi \overline{K}^{*0}$ decays have been measured. The results are

$$\mathcal{B}(B_s^0 \to J/\psi \overline{K}^{*0}) = (4.14 \pm 0.18(\text{stat}) \pm 0.26(\text{syst}) \pm 0.24(f_d/f_s)) \times 10^{-5}$$

$$f_0 = 0.497 \pm 0.025(\text{stat}) \pm 0.025(\text{syst})$$

$$f_\| = 0.179 \pm 0.027(\text{stat}) \pm 0.013(\text{syst})$$

$$A_0^{CP}(B_s^0 \to J/\psi \overline{K}^{*0}) = -0.048 \pm 0.057(\text{stat}) \pm 0.020(\text{syst})$$

$$A_\|^{CP}(B_s^0 \to J/\psi \overline{K}^{*0}) = 0.171 \pm 0.152(\text{stat}) \pm 0.028(\text{syst})$$

$$A_\perp^{CP}(B_s^0 \to J/\psi \overline{K}^{*0}) = -0.049 \pm 0.096(\text{stat}) \pm 0.025(\text{syst}),$$

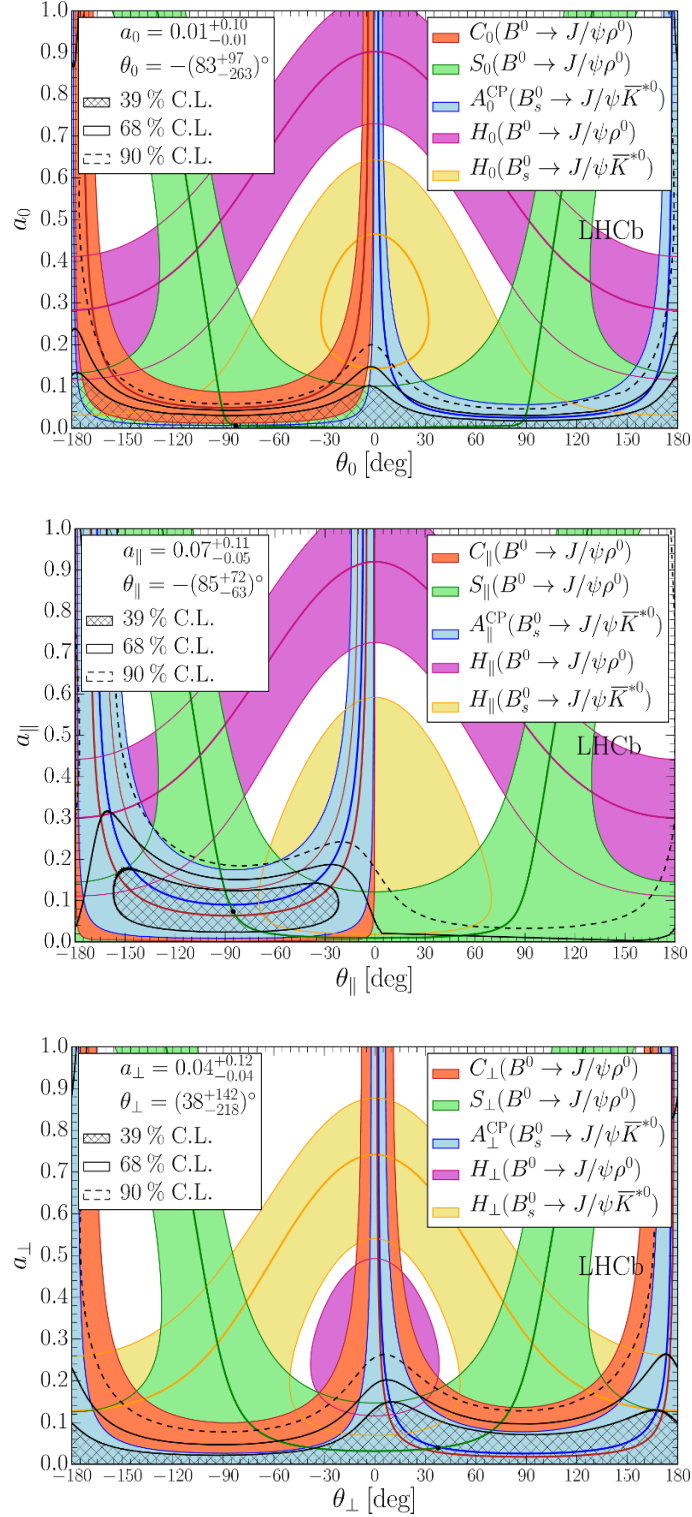**Figure 8**. Limits on the penguin parameters a_i and θ_i obtained from intersecting contours derived from the CP asymmetries and branching fraction information in $B_s^0 \to J/\psi \overline{K}^{*0}$ and $B^0 \to J/\psi \rho^0$. Superimposed are the confidence level contours obtained from a χ^2 fit to the data. The longitudinal (top), parallel (middle) and perpendicular (bottom) polarisations are shown.

which supersede those of ref. [16], with precision improved by a factor of 2–3. The shift on ϕ_s due to penguin pollution is estimated from a combination with the $B^0 \to J/\psi\,\rho^0$ channel [15], and is found be to compatible with the result from the earlier analysis.

Acknowledgments

A Angular acceptance

To take into account angular acceptance effects, ten normalisation weights, ξ_{ij}, are computed and embedded in the normalization integral of the angular distribution given in eq. (6.1) following the procedure described in ref. [57]. Using the transversity amplitude basis, the fitting PDF can be written as

$$\frac{d\Gamma(\theta_K, \theta_\mu, \varphi_h)}{d\Omega} = \frac{\sum_i \sum_{j \leq i} \mathcal{R}e[A_i A_j^* \, F_{ij}(\theta_K, \theta_\mu, \varphi_h)]}{\sum_k \sum_{l \leq k} \mathcal{R}e[A_k A_l^* \int F_{kl}(\theta_K', \theta_\mu', \varphi_h') \, \epsilon_\Omega(\theta_K', \theta_\mu', \varphi_h') \, d\Omega']}, \qquad (A.1)$$

where the real or imaginary angular functions $F_{ij}(\theta_K, \theta_\mu, \varphi_h)$ are obtained when combining eq. (6.1) and eqs. (6.2)–(6.5), and where $\epsilon_\Omega(\theta_K, \theta_\mu, \varphi_h)$ denotes the angular acceptance. The normalization weights correspond to the integrals

$$\xi_{ij} = \begin{cases} \int \mathcal{R}e[F_{ij}(\theta_K, \theta_\mu, \varphi_h)] \, \epsilon_\Omega(\theta_K, \theta_\mu, \varphi_h) \, d\Omega, & \text{if } F_{ij} \in \mathbb{R}, \\ \int \mathcal{I}m[F_{ij}(\theta_K, \theta_\mu, \varphi_h)] \, \epsilon_\Omega(\theta_K, \theta_\mu, \varphi_h) \, d\Omega, & \text{if } F_{ij} \in \mathbb{I}. \end{cases} \qquad (A.2)$$

In the absence of acceptance effects, the normalisation weights related to the interference terms are equal to zero by definition, whereas those related to each polarisation amplitude squared are equal to unity. Eight sets of normalisation weights are calculated separately, one for each $m_{K^- \pi^+}$ bin and kaon charge.

	ij	ξ_{ij}/ξ_{00}
1	(00)	1.000
2	($\parallel\parallel$)	$+1.379 \pm 0.029$
3	($\perp\perp$)	$+1.388 \pm 0.030$
4	($\parallel\perp$)	$+0.035 \pm 0.019$
5	(0$\parallel$)	-0.003 ± 0.012
6	(0$\perp$)	$+0.010 \pm 0.011$
7	(SS)	$+1.190 \pm 0.019$
8	(S$\parallel$)	-0.042 ± 0.017
9	(S$\perp$)	$+0.029 \pm 0.016$
10	(S0)	-0.929 ± 0.024

Table 6. Corrected angular acceptance weights for $K^-\pi^+$ events lying in the first $m_{K^-\pi^+}$ bin. The ξ_{ij} weights are normalised with respect to the ξ_{00} weight.

In order to correct both for imperfections in the detector simulation and for the absence of any S-wave component in the simulation sample, the weights are refined using an iterative procedure where the angular acceptance is re-evaluated recursively until it does not change significantly. Table 6 gives one set of normalisation weights after the iterative procedure. The effect of this correction is below one standard deviation for all the normalisation weights except for the (S0) weight. This is expected due to the rapid efficiency drop close to $\cos\theta_K = 1$ which directly impacts the (S0) weight. At each step of this procedure the simulation sample is corrected both for the absence of an S-wave component and for the imperfections in the detector simulation. For the first correction, the angular fit result to data is used, whereas for the second the kaon and muon track momentum distributions of data are used. In both cases the correction is implemented by assigning weights to each event of the simulation sample.

B Correlation matrix

The statistical-only correlation matrix of the angular parameters obtained from the fit to data, as described in section 8.1, is given in table 7. Here, the superscript $l = 0, 1, 2, 3$ in F_S^l and δ_S^l represent the number of the $m_{K^-\pi^+}$ bin as defined in table 2.

	A_0^{CP}	A_S^{CP}	$A_\parallel^{CP}$	$A_\perp^{CP}$	F_S^0	F_S^1	F_S^2	F_S^3	$\delta_\parallel$	$\delta_\perp$	δ_S^0	δ_S^1	δ_S^2	δ_S^3	f_0	$f_\parallel$
A_0^{CP}	+1.00	-0.12	-0.11	-0.17	-0.13	-0.02	-0.06	-0.01	$+0.03$	$+0.02$	$+0.10$	-0.00	$+0.07$	$+0.01$	$+0.06$	-0.05
A_S^{CP}		$+1.00$	-0.14	-0.12	$+0.16$	-0.12	$+0.03$	-0.10	$+0.00$	-0.06	$+0.02$	$+0.07$	$+0.05$	$+0.07$	$+0.01$	$+0.03$
$A_\parallel^{CP}$			$+1.00$	-0.49	$+0.02$	$+0.09$	-0.02	$+0.08$	$+0.09$	$+0.06$	-0.06	-0.04	-0.05	-0.12	-0.04	-0.07
$A_\perp^{CP}$				$+1.00$	-0.00	-0.01	-0.06	-0.07	-0.09	-0.03	-0.03	$+0.01$	-0.02	$+0.07$	$+0.01$	-0.06
F_S^0					$+1.00$	$+0.01$	-0.01	-0.03	-0.10	-0.24	-0.77	$+0.01$	$+0.04$	-0.00	$+0.10$	-0.09
F_S^1						$+1.00$	-0.01	-0.00	-0.02	-0.05	-0.01	-0.25	$+0.03$	-0.01	$+0.15$	-0.10
F_S^2							$+1.00$	$+0.01$	-0.04	$+0.07$	$+0.01$	-0.00	-0.22	$+0.00$	-0.02	$+0.04$
F_S^3								$+1.00$	$+0.08$	$+0.08$	$+0.00$	-0.01	-0.03	-0.29	-0.09	$+0.04$
$\delta_\parallel$									$+1.00$	$+0.62$	$+0.10$	$+0.14$	$+0.03$	$+0.11$	$+0.04$	-0.03
$\delta_\perp$										$+1.00$	$+0.17$	$+0.13$	-0.02	$+0.13$	$+0.05$	-0.04
δ_S^0											$+1.00$	$+0.04$	$+0.03$	$+0.04$	$+0.08$	$+0.04$
δ_S^1												$+1.00$	$+0.04$	$+0.04$	$+0.13$	-0.05
δ_S^2													$+1.00$	$+0.04$	$+0.27$	-0.08
δ_S^3														$+1.00$	$+0.11$	$+0.00$
f_0															$+1.00$	-0.34
$f_\parallel$																$+1.00$

Table 7. Statistical correlation matrix for the parameters from the angular fit.

References

[1] M. Kobayashi and T. Maskawa, *CP Violation in the Renormalizable Theory of Weak Interaction*, *Prog. Theor. Phys.* **49** (1973) 652 [INSPIRE].

[2] W. Altmannshofer, A.J. Buras, S. Gori, P. Paradisi and D.M. Straub, *Anatomy and Phenomenology of FCNC and CPV Effects in SUSY Theories*, *Nucl. Phys.* **B 830** (2010) 17 [arXiv:0909.1333] [INSPIRE].

[3] W. Altmannshofer, A.J. Buras and D. Guadagnoli, *The MFV limit of the MSSM for low* $\tan\beta$: *Meson mixings revisited*, *JHEP* **11** (2007) 065 [hep-ph/0703200] [INSPIRE].

[4] A.J. Buras, *Flavour Theory: 2009*, PoS(EPS-HEP 2009)024 [arXiv:0910.1032] [INSPIRE].

[5] C.-W. Chiang, A. Datta, M. Duraisamy, D. London, M. Nagashima and A. Szynkman, *New Physics in* $B_s^0 \to J/\psi\phi$: *A General Analysis*, *JHEP* **04** (2010) 031 [arXiv:0910.2929] [INSPIRE].

[6] CKMFITTER GROUP collaboration, J. Charles et al., *Current status of the Standard Model CKM fit and constraints on* $\Delta F = 2$ *New Physics*, *Phys. Rev.* **D 91** (2015) 073007 [arXiv:1501.05013] [INSPIRE].

[7] HEAVY FLAVOR AVERAGING GROUP (HFAG) collaboration, Y. Amhis et al., *Averages of b-hadron, c-hadron and* τ-*lepton properties as of summer 2014*, arXiv:1412.7515 [INSPIRE] and updated results and plots available at http://www.slac.stanford.edu/xorg/hfag/.

[8] LHCb collaboration, *Precision measurement of CP violation in* $B_s^0 \to J/\psi K^+ K^-$ *decays*, *Phys. Rev. Lett.* **114** (2015) 041801 [arXiv:1411.3104] [INSPIRE].

[9] R. Fleischer, *Extracting CKM phases from angular distributions of* $B_{(d,s)}$ *decays into admixtures of CP eigenstates*, *Phys. Rev.* **D 60** (1999) 073008 [hep-ph/9903540] [INSPIRE].

[10] R. Fleischer, *In Pursuit of New Physics in the B System*, *Nucl. Phys. Proc. Suppl.* **163** (2007) 171 [hep-ph/0607241] [INSPIRE].

[11] S. Faller, R. Fleischer and T. Mannel, *Precision Physics with* $B_s^0 \to J/\psi\phi$ *at the LHC: The Quest for New Physics*, *Phys. Rev.* **D 79** (2009) 014005 [arXiv:0810.4248] [INSPIRE].

[12] X. Liu, W. Wang and Y. Xie, *Penguin pollution in* $B \to J/\psi V$ *decays and impact on the extraction of the* $B_s - \bar{B}_s$ *mixing phase*, *Phys. Rev.* **D 89** (2014) 094010 [arXiv:1309.0313] [INSPIRE].

[13] K. De Bruyn and R. Fleischer, *A roadmap to control penguin effects in* $B_d^0 \to J/\psi K_S^0$ *and* $B_s^0 \to J/\psi\phi$, *JHEP* **03** (2015) 145 [arXiv:1412.6834] [INSPIRE].

[14] P. Frings, U. Nierste and M. Wiebusch, *Penguin contributions to CP phases in* $B_{d,s}$ *decays to charmonium*, *Phys. Rev. Lett.* **115** (2015) 061802 [arXiv:1503.00859] [INSPIRE].

[15] LHCb collaboration, *Measurement of the CP-violating phase* β *in* $\overline{B}^0 \to J/\psi\pi^+\pi^-$ *decays and limits on penguin effects*, *Phys. Lett.* **B 742** (2015) 38 [arXiv:1411.1634] [INSPIRE].

[16] LHCb collaboration, *Measurement of the* $B_s^0 \to J/\psi\overline{K}^{*0}$ *branching fraction and angular amplitudes*, *Phys. Rev.* **D 86** (2012) 071102(R) [arXiv:1208.0738] [INSPIRE].

[17] M. Pivk and F.R. Le Diberder, *SPlot: A Statistical tool to unfold data distributions*, *Nucl. Instrum. Meth.* **A 555** (2005) 356 [physics/0402083] [INSPIRE].

[18] LHCb collaboration, *LHCb Detector Performance*, *Int. J. Mod. Phys.* **A 30** (2015) 1530022 [arXiv:1412.6352] [INSPIRE].

[19] LHCb collaboration, *The LHCb Detector at the LHC*, 2008 *JINST* **3** S08005 [ɪɴSPIRE].

[20] T. Sjöstrand, S. Mrenna and P.Z. Skands, *PYTHIA 6.4 Physics and Manual*, *JHEP* **05** (2006) 026 [hep-ph/0603175] [ɪɴSPIRE].

[21] T. Sjöstrand, S. Mrenna and P.Z. Skands, *A Brief Introduction to PYTHIA 8.1*, *Comput. Phys. Commun.* **178** (2008) 852 [arXiv:0710.3820] [ɪɴSPIRE].

[22] LHCb collaboration, *Handling of the generation of primary events in Gauss, the LHCb simulation framework*, *J. Phys. Conf. Ser.* **331** (2011) 032047 [ɪɴSPIRE].

[23] D.J. Lange, *The EvtGen particle decay simulation package*, *Nucl. Instrum. Meth.* **A 462** (2001) 152 [ɪɴSPIRE].

[24] P. Golonka and Z. Was, *PHOTOS Monte Carlo: A Precision tool for QED corrections in Z and W decays*, *Eur. Phys. J.* **C 45** (2006) 97 [hep-ph/0506026] [ɪɴSPIRE].

[25] GEANT4 collaboration, J. Allison et al., *Geant4 developments and applications*, *IEEE Trans. Nucl. Sci.* **53** (2006) 270 [ɪɴSPIRE].

[26] GEANT4 collaboration, S. Agostinelli et al., *Geant4: A Simulation toolkit*, *Nucl. Instrum. Meth.* **A 506** (2003) 250 [ɪɴSPIRE].

[27] M. Clemencic et al., *The LHCb simulation application, Gauss: Design, evolution and experience*, *J. Phys. Conf. Ser.* **331** (2011) 032023 [ɪɴSPIRE].

[28] L. Breiman, J.H. Friedman, R.A. Olshen and C.J. Stone, *Classification and regression trees*, Wadsworth international group, Belmont California U.S.A. (1984).

[29] R.E. Schapire and Y. Freund, *A decision-theoretic generalization of on-line learning and an application to boosting*, *J. Comput. Syst. Sci.* **55** (1997) 119 [ɪɴSPIRE].

[30] PARTICLE DATA GROUP collaboration, K.A. Olive et al., *Review of Particle Physics*, *Chin. Phys.* **C 38** (2014) 090001 [ɪɴSPIRE].

[31] LHCb collaboration, *Evidence for pentaquark-charmonium states in $\Lambda_b^0 \to J/\psi p K^-$ decays*, *Phys. Rev. Lett.* **115** (2015) 072001 [arXiv:1507.03414] [ɪɴSPIRE].

[32] LHCb collaboration, *Amplitude analysis and branching fraction measurement of $\overline{B}_s^0 \to J/\psi K^+ K^-$*, *Phys. Rev.* **D 87** (2013) 072004 [arXiv:1302.1213] [ɪɴSPIRE].

[33] LHCb collaboration, *Measurement of resonant and CP components in $\overline{B}_s^0 \to J/\psi \pi^+ \pi^-$ decays*, *Phys. Rev.* **D 89** (2014) 092006 [arXiv:1402.6248] [ɪɴSPIRE].

[34] LHCb collaboration, *Measurement of the resonant and CP components in $\overline{B}^0 \to J/\psi \pi^+ \pi^-$ decays*, *Phys. Rev.* **D 90** (2014) 012003 [arXiv:1404.5673] [ɪɴSPIRE].

[35] LHCb collaboration, *Observation of the $\Lambda_b^0 \to J/\psi p \pi^-$ decay*, *JHEP* **07** (2014) 103 [arXiv:1406.0755] [ɪɴSPIRE].

[36] L. Amoroso, *Ricerche intorno alla curve dei redditi*, *Ann. Mat. Pur. Appl.* **21** (1925) 123.

[37] D. Martinez Santos and F. Dupertuis, *Mass distributions marginalized over per-event errors*, *Nucl. Instrum. Meth.* **A 764** (2014) 150 [arXiv:1312.5000] [ɪɴSPIRE].

[38] L. Zhang and S. Stone, *Time-dependent Dalitz-plot formalism for $B \to J/\psi h^+ h^-$*, *Phys. Lett.* **B 719** (2013) 383 [arXiv:1212.6434] [ɪɴSPIRE].

[39] D. Aston et al., *A study of $K^- \pi^+$ scattering in the reaction $K^- p \to K^- \pi^+ n$ at 11 GeV/c*, *Nucl. Phys.* **B 296** (1988) 493 [ɪɴSPIRE].

[40] D. Herndon, P. Soding and R.J. Cashmore, *A generalised isobar model formalism*, [*Phys. Rev.* **D 11** (1975) 3165](#) [[INSPIRE](#)].

[41] LHCb collaboration, *First evidence of direct CP violation in charmless two-body decays of B_s^0 mesons*, [*Phys. Rev. Lett.* **108** (2012) 201601](#) [[arXiv:1202.6251](#)] [[INSPIRE](#)].

[42] LHCb collaboration, *First observation of CP violation in the decays of B_s^0 mesons*, [*Phys. Rev. Lett.* **110** (2013) 221601](#) [[arXiv:1304.6173](#)] [[INSPIRE](#)].

[43] LHCb collaboration, *Measurement of the $\overline{B}^0$–B^0 and $\overline{B}_s^0$–B_s^0 production asymmetries in pp collisions at $\sqrt{s} = 7\,TeV$*, [*Phys. Lett.* **B 739** (2014) 218](#) [[arXiv:1408.0275](#)] [[INSPIRE](#)].

[44] LHCb collaboration, *Measurement of the semileptonic CP asymmetry in B^0–$\overline{B}^0$ mixing*, [*Phys. Rev. Lett.* **114** (2015) 041601](#) [[arXiv:1409.8586](#)] [[INSPIRE](#)].

[45] LHCb collaboration, *Measurement of CP asymmetry in $D^0 \to K^- K^+$ and $D^0 \to \pi^- \pi^+$ decays*, [*JHEP* **07** (2014) 041](#) [[arXiv:1405.2797](#)] [[INSPIRE](#)].

[46] BELLE collaboration, K. Abe et al., *Measurements of branching fractions and decay amplitudes in $B \to J/\psi K^*$ decays*, [*Phys. Lett.* **B 538** (2002) 11](#) [[hep-ex/0205021](#)] [[INSPIRE](#)].

[47] LHCb collaboration, *Measurement of the polarization amplitudes in $B^0 \to J/\psi K^*(892)^0$ decays*, [*Phys. Rev.* **D 88** (2013) 052002](#) [[arXiv:1307.2782](#)] [[INSPIRE](#)].

[48] I.J.R. Aitchison, *K-matrix formalism for overlapping resonances*, [*Nucl. Phys.* **A 189** (1972) 417](#) [[INSPIRE](#)].

[49] M. Gronau, O.F. Hernandez, D. London and J.L. Rosner, *Broken* SU(3) *symmetry in two-body B decays*, [*Phys. Rev.* **D 52** (1995) 6356](#) [[hep-ph/9504326](#)] [[INSPIRE](#)].

[50] LHCb collaboration, *First observation of $\overline{B}^0 \to J/\psi K^+ K^-$ and search for $\overline{B}^0 \to J/\psi \phi$ decays*, [*Phys. Rev.* **D 88** (2013) 072005](#) [[arXiv:1308.5916](#)] [[INSPIRE](#)].

[51] K. De Bruyn, R. Fleischer, R. Knegjens, P. Koppenburg, M. Merk and N. Tuning, *Branching Ratio Measurements of B_s Decays*, [*Phys. Rev.* **D 86** (2012) 014027](#) [[arXiv:1204.1735](#)] [[INSPIRE](#)].

[52] K. De Bruyn, *Searching for penguin footprints: Towards high precision CP violation measurements in the B meson systems*, Ph.D. Thesis, VU University, Amsterdam The Netherlands (2015) [[CERN-THESIS-2015-126](#)].

[53] A.S. Dighe, I. Dunietz and R. Fleischer, *Extracting CKM phases and B_s^0–$\overline{B}_s^0$ mixing parameters from angular distributions of non-leptonic B decays*, [*Eur. Phys. J.* **C 6** (1999) 647](#) [[hep-ph/9804253](#)] [[INSPIRE](#)].

[54] A. Bharucha, D.M. Straub and R. Zwicky, *$B \to V \ell^+ \ell^-$ in the Standard Model from light-cone sum rules*, [arXiv:1503.05534](#) [[INSPIRE](#)].

[55] LHCb collaboration, *Measurement of CP violation in $B^0 \to J/\psi K_S^0$ decays*, [*Phys. Rev. Lett.* **115** (2015) 031601](#) [[arXiv:1503.07089](#)] [[INSPIRE](#)].

[56] LHCb collaboration, *Measurement of the time-dependent CP asymmetries in $B_s^0 \to J/\psi K_S^0$*, [*JHEP* **06** (2015) 131](#) [[arXiv:1503.07055](#)] [[INSPIRE](#)].

[57] T. du Pree, *Search for a strange phase in beautiful oscillations*, Ph.D. Thesis, VU University, Amsterdam The Netherlands (2010) [[CERN-THESIS-2010-124](#)] [[INSPIRE](#)].

The LHCb collaboration

R. Aaij[38], B. Adeva[37], M. Adinolfi[46], A. Affolder[52], Z. Ajaltouni[5], S. Akar[6], J. Albrecht[9],
F. Alessio[38], M. Alexander[51], S. Ali[41], G. Alkhazov[30], P. Alvarez Cartelle[53], A.A. Alves Jr[57],
S. Amato[2], S. Amerio[22], Y. Amhis[7], L. An[3], L. Anderlini[17], J. Anderson[40], G. Andreassi[39],
M. Andreotti[16,f], J.E. Andrews[58], R.B. Appleby[54], O. Aquines Gutierrez[10], F. Archilli[38],
P. d'Argent[11], A. Artamonov[35], M. Artuso[59], E. Aslanides[6], G. Auriemma[25,m], M. Baalouch[5],
S. Bachmann[11], J.J. Back[48], A. Badalov[36], C. Baesso[60], W. Baldini[16,38], R.J. Barlow[54],
C. Barschel[38], S. Barsuk[7], W. Barter[38], V. Batozskaya[28], V. Battista[39], A. Bay[39], L. Beaucourt[4],
J. Beddow[51], F. Bedeschi[23], I. Bediaga[1], L.J. Bel[41], V. Bellee[39], N. Belloli[20,j], I. Belyaev[31],
E. Ben-Haim[8], G. Bencivenni[18], S. Benson[38], J. Benton[46], A. Berezhnoy[32], R. Bernet[40],
A. Bertolin[22], M.-O. Bettler[38], M. van Beuzekom[41], A. Bien[11], S. Bifani[45], P. Billoir[8], T. Bird[54],
A. Birnkraut[9], A. Bizzeti[17,h], T. Blake[48], F. Blanc[39], J. Blouw[10], S. Blusk[59], V. Bocci[25],
A. Bondar[34], N. Bondar[30,38], W. Bonivento[15], S. Borghi[54], M. Borsato[7], T.J.V. Bowcock[52],
E. Bowen[40], C. Bozzi[16], S. Braun[11], M. Britsch[10], T. Britton[59], J. Brodzicka[54], N.H. Brook[46],
E. Buchanan[46], A. Bursche[40], J. Buytaert[38], S. Cadeddu[15], R. Calabrese[16,f], M. Calvi[20,j],
M. Calvo Gomez[36,o], P. Campana[18], D. Campora Perez[38], L. Capriotti[54], A. Carbone[14,d],
G. Carboni[24,k], R. Cardinale[19,i], A. Cardini[15], P. Carniti[20,j], L. Carson[50], K. Carvalho Akiba[2,38],
G. Casse[52], L. Cassina[20,j], L. Castillo Garcia[38], M. Cattaneo[38], Ch. Cauet[9], G. Cavallero[19],
R. Cenci[23,s], M. Charles[8], Ph. Charpentier[38], M. Chefdeville[4], S. Chen[54], S.-F. Cheung[55],
N. Chiapolini[40], M. Chrzaszcz[40], X. Cid Vidal[38], G. Ciezarek[41], P.E.L. Clarke[50], M. Clemencic[38],
H.V. Cliff[47], J. Closier[38], V. Coco[38], J. Cogan[6], E. Cogneras[5], V. Cogoni[15,e], L. Cojocariu[29],
G. Collazuol[22], P. Collins[38], A. Comerma-Montells[11], A. Contu[15], A. Cook[46], M. Coombes[46],
S. Coquereau[8], G. Corti[38], M. Corvo[16,f], B. Couturier[38], G.A. Cowan[50], D.C. Craik[48],
A. Crocombe[48], M. Cruz Torres[60], S. Cunliffe[53], R. Currie[53], C. D'Ambrosio[38], E. Dall'Occo[41],
J. Dalseno[46], P.N.Y. David[41], A. Davis[57], K. De Bruyn[6], S. De Capua[54], M. De Cian[11],
J.M. De Miranda[1], L. De Paula[2], P. De Simone[18], C.-T. Dean[51], D. Decamp[4], M. Deckenhoff[9],
L. Del Buono[8], N. Déléage[4], M. Demmer[9], D. Derkach[65], O. Deschamps[5], F. Dettori[38], B. Dey[21],
A. Di Canto[38], F. Di Ruscio[24], H. Dijkstra[38], S. Donleavy[52], F. Dordei[11], M. Dorigo[39],
A. Dosil Suárez[37], D. Dossett[48], A. Dovbnya[43], K. Dreimanis[52], L. Dufour[41], G. Dujany[54],
F. Dupertuis[39], P. Durante[38], R. Dzhelyadin[35], A. Dziurda[26], A. Dzyuba[30], S. Easo[49,38],
U. Egede[53], V. Egorychev[31], S. Eidelman[34], S. Eisenhardt[50], U. Eitschberger[9], R. Ekelhof[9],
L. Eklund[51], I. El Rifai[5], Ch. Elsasser[40], S. Ely[59], S. Esen[11], H.M. Evans[47], T. Evans[55],
A. Falabella[14], C. Färber[38], N. Farley[45], S. Farry[52], R. Fay[52], D. Ferguson[50],
V. Fernandez Albor[37], F. Ferrari[14], F. Ferreira Rodrigues[1], M. Ferro-Luzzi[38], S. Filippov[33],
M. Fiore[16,38,f], M. Fiorini[16,f], M. Firlej[27], C. Fitzpatrick[39], T. Fiutowski[27], K. Fohl[38], P. Fol[53],
M. Fontana[15], F. Fontanelli[19,i], R. Forty[38], O. Francisco[2], M. Frank[38], C. Frei[38], M. Frosini[17],
J. Fu[21], E. Furfaro[24,k], A. Gallas Torreira[37], D. Galli[14,d], S. Gallorini[22], S. Gambetta[50],
M. Gandelman[2], P. Gandini[55], Y. Gao[3], J. García Pardiñas[37], J. Garra Tico[47], L. Garrido[36],
D. Gascon[36], C. Gaspar[38], R. Gauld[55], L. Gavardi[9], G. Gazzoni[5], D. Gerick[11], E. Gersabeck[11],
M. Gersabeck[54], T. Gershon[48], Ph. Ghez[4], S. Gianì[39], V. Gibson[47], O. G. Girard[39], L. Giubega[29],
V.V. Gligorov[38], C. Göbel[60], D. Golubkov[31], A. Golutvin[53,31,38], A. Gomes[1,a], C. Gotti[20,j],
M. Grabalosa Gándara[5], R. Graciani Diaz[36], L.A. Granado Cardoso[38], E. Graugés[36],
E. Graverini[40], G. Graziani[17], A. Grecu[29], E. Greening[55], S. Gregson[47], P. Griffith[45], L. Grillo[11],
O. Grünberg[63], B. Gui[59], E. Gushchin[33], Yu. Guz[35,38], T. Gys[38], T. Hadavizadeh[55],
C. Hadjivasiliou[59], G. Haefeli[39], C. Haen[38], S.C. Haines[47], S. Hall[53], B. Hamilton[58], X. Han[11],
S. Hansmann-Menzemer[11], N. Harnew[55], S.T. Harnew[46], J. Harrison[54], J. He[38], T. Head[39],
V. Heijne[41], K. Hennessy[52], P. Henrard[5], L. Henry[8], E. van Herwijnen[38], M. Heß[63], A. Hicheur[2],
D. Hill[55], M. Hoballah[5], C. Hombach[54], W. Hulsbergen[41], T. Humair[53], N. Hussain[55],

D. Hutchcroft[52], D. Hynds[51], M. Idzik[27], P. Ilten[56], R. Jacobsson[38], A. Jaeger[11], J. Jalocha[55],
E. Jans[41], A. Jawahery[58], F. Jing[3], M. John[55], D. Johnson[38], C.R. Jones[47], C. Joram[38],
B. Jost[38], N. Jurik[59], S. Kandybei[43], W. Kanso[6], M. Karacson[38], T.M. Karbach[38,†], S. Karodia[51],
M. Kecke[11], M. Kelsey[59], I.R. Kenyon[45], M. Kenzie[38], T. Ketel[42], B. Khanji[20,38,j],
C. Khurewathanakul[39], S. Klaver[54], K. Klimaszewski[28], O. Kochebina[7], M. Kolpin[11],
I. Komarov[39], R.F. Koopman[42], P. Koppenburg[41,38], M. Kozeiha[5], L. Kravchuk[33], K. Kreplin[11],
M. Kreps[48], G. Krocker[11], P. Krokovny[34], F. Kruse[9], W. Krzemien[28], W. Kucewicz[26,n],
M. Kucharczyk[26], V. Kudryavtsev[34], A. K. Kuonen[39], K. Kurek[28], T. Kvaratskheliya[31],
D. Lacarrere[38], G. Lafferty[54], A. Lai[15], D. Lambert[50], G. Lanfranchi[18], C. Langenbruch[48],
B. Langhans[38], T. Latham[48], C. Lazzeroni[45], R. Le Gac[6], J. van Leerdam[41], J.-P. Lees[4],
R. Lefèvre[5], A. Leflat[32,38], J. Lefrançois[7], E. Lemos Cid[37], O. Leroy[6], T. Lesiak[26],
B. Leverington[11], Y. Li[7], T. Likhomanenko[65,64], M. Liles[52], R. Lindner[38], C. Linn[38],
F. Lionetto[40], B. Liu[15], X. Liu[3], D. Loh[48], I. Longstaff[51], J.H. Lopes[2], D. Lucchesi[22,q],
M. Lucio Martinez[37], H. Luo[50], A. Lupato[22], E. Luppi[16,f], O. Lupton[55], A. Lusiani[23],
F. Machefert[7], F. Maciuc[29], O. Maev[30], K. Maguire[54], S. Malde[55], A. Malinin[64], G. Manca[7],
G. Mancinelli[6], P. Manning[59], A. Mapelli[38], J. Maratas[5], J.F. Marchand[4], U. Marconi[14],
C. Marin Benito[36], P. Marino[23,38,s], J. Marks[11], G. Martellotti[25], M. Martin[6], M. Martinelli[39],
D. Martinez Santos[37], F. Martinez Vidal[66], D. Martins Tostes[2], A. Massafferri[1], R. Matev[38],
A. Mathad[48], Z. Mathe[38], C. Matteuzzi[20], A. Mauri[40], B. Maurin[39], A. Mazurov[45],
M. McCann[53], J. McCarthy[45], A. McNab[54], R. McNulty[12], B. Meadows[57], F. Meier[9],
M. Meissner[11], D. Melnychuk[28], M. Merk[41], E Michielin[22], D.A. Milanes[62], M.-N. Minard[4],
D.S. Mitzel[11], J. Molina Rodriguez[60], I.A. Monroy[62], S. Monteil[5], M. Morandin[22], P. Morawski[27],
A. Mordà[6], M.J. Morello[23,s], J. Moron[27], A.B. Morris[50], R. Mountain[59], F. Muheim[50],
D. Müller[54], J. Müller[9], K. Müller[40], V. Müller[9], M. Mussini[14], B. Muster[39], P. Naik[46],
T. Nakada[39], R. Nandakumar[49], A. Nandi[55], I. Nasteva[2], M. Needham[50], N. Neri[21], S. Neubert[11],
N. Neufeld[38], M. Neuner[11], A.D. Nguyen[39], T.D. Nguyen[39], C. Nguyen-Mau[39,p], V. Niess[5],
R. Niet[9], N. Nikitin[32], T. Nikodem[11], A. Novoselov[35], D.P. O'Hanlon[48], A. Oblakowska-Mucha[27],
V. Obraztsov[35], S. Ogilvy[51], O. Okhrimenko[44], R. Oldeman[15,e], C.J.G. Onderwater[67],
B. Osorio Rodrigues[1], J.M. Otalora Goicochea[2], A. Otto[38], P. Owen[53], A. Oyanguren[66],
A. Palano[13,c], F. Palombo[21,t], M. Palutan[18], J. Panman[38], A. Papanestis[49], M. Pappagallo[51],
L.L. Pappalardo[16,f], C. Pappenheimer[57], C. Parkes[54], G. Passaleva[17], G.D. Patel[52], M. Patel[53],
C. Patrignani[19,i], A. Pearce[54,49], A. Pellegrino[41], G. Penso[25,l], M. Pepe Altarelli[38],
S. Perazzini[14,d], P. Perret[5], L. Pescatore[45], K. Petridis[46], A. Petrolini[19,i], M. Petruzzo[21],
E. Picatoste Olloqui[36], B. Pietrzyk[4], T. Pilař[48], D. Pinci[25], A. Pistone[19], A. Piucci[11],
S. Playfer[50], M. Plo Casasus[37], T. Poikela[38], F. Polci[8], A. Poluektov[48,34], I. Polyakov[31],
E. Polycarpo[2], A. Popov[35], D. Popov[10,38], B. Popovici[29], C. Potterat[2], E. Price[46], J.D. Price[52],
J. Prisciandaro[39], A. Pritchard[52], C. Prouve[46], V. Pugatch[44], A. Puig Navarro[39], G. Punzi[23,r],
W. Qian[4], R. Quagliani[7,46], B. Rachwal[26], J.H. Rademacker[46], M. Rama[23], M.S. Rangel[2],
I. Raniuk[43], N. Rauschmayr[38], G. Raven[42], F. Redi[53], S. Reichert[54], M.M. Reid[48], A.C. dos Reis[1],
S. Ricciardi[49], S. Richards[46], M. Rihl[38], K. Rinnert[52], V. Rives Molina[36], P. Robbe[7,38],
A.B. Rodrigues[1], E. Rodrigues[54], J.A. Rodriguez Lopez[62], P. Rodriguez Perez[54], S. Roiser[38],
V. Romanovsky[35], A. Romero Vidal[37], J. W. Ronayne[12], M. Rotondo[22], J. Rouvinet[39], T. Ruf[38],
P. Ruiz Valls[66], J.J. Saborido Silva[37], N. Sagidova[30], P. Sail[51], B. Saitta[15,e],
V. Salustino Guimaraes[2], C. Sanchez Mayordomo[66], B. Sanmartin Sedes[37], R. Santacesaria[25],
C. Santamarina Rios[37], M. Santimaria[18], E. Santovetti[24,k], A. Sarti[18,l], C. Satriano[25,m],
A. Satta[24], D.M. Saunders[46], D. Savrina[31,32], M. Schiller[38], H. Schindler[38], M. Schlupp[9],
M. Schmelling[10], T. Schmelzer[9], B. Schmidt[38], O. Schneider[39], A. Schopper[38], M. Schubiger[39],
M.-H. Schune[7], R. Schwemmer[38], B. Sciascia[18], A. Sciubba[25,l], A. Semennikov[31], N. Serra[40],
J. Serrano[6], L. Sestini[22], P. Seyfert[20], M. Shapkin[35], I. Shapoval[16,43,f], Y. Shcheglov[30],

T. Shears[52], L. Shekhtman[34], V. Shevchenko[64], A. Shires[9], B.G. Siddi[16], R. Silva Coutinho[48,40],
L. Silva de Oliveira[2], G. Simi[22], M. Sirendi[47], N. Skidmore[46], T. Skwarnicki[59], E. Smith[55,49],
E. Smith[53], I. T. Smith[50], J. Smith[47], M. Smith[54], H. Snoek[41], M.D. Sokoloff[57,38], F.J.P. Soler[51],
F. Soomro[39], D. Souza[46], B. Souza De Paula[2], B. Spaan[9], P. Spradlin[51], S. Sridharan[38],
F. Stagni[38], M. Stahl[11], S. Stahl[38], S. Stefkova[53], O. Steinkamp[40], O. Stenyakin[35], S. Stevenson[55],
S. Stoica[29], S. Stone[59], B. Storaci[40], S. Stracka[23,s], M. Straticiuc[29], U. Straumann[40], L. Sun[57],
W. Sutcliffe[53], K. Swientek[27], S. Swientek[9], V. Syropoulos[42], M. Szczekowski[28], P. Szczypka[39,38],
T. Szumlak[27], S. T'Jampens[4], A. Tayduganov[6], T. Tekampe[9], M. Teklishyn[7], G. Tellarini[16,f],
F. Teubert[38], C. Thomas[55], E. Thomas[38], J. van Tilburg[41], V. Tisserand[4], M. Tobin[39], J. Todd[57],
S. Tolk[42], L. Tomassetti[16,f], D. Tonelli[38], S. Topp-Joergensen[55], N. Torr[55], E. Tournefier[4],
S. Tourneur[39], K. Trabelsi[39], M.T. Tran[39], M. Tresch[40], A. Trisovic[38], A. Tsaregorodtsev[6],
P. Tsopelas[41], N. Tuning[41,38], A. Ukleja[28], A. Ustyuzhanin[65,64], U. Uwer[11], C. Vacca[15,e],
V. Vagnoni[14], G. Valenti[14], A. Vallier[7], R. Vazquez Gomez[18], P. Vazquez Regueiro[37],
C. Vázquez Sierra[37], S. Vecchi[16], J.J. Velthuis[46], M. Veltri[17,g], G. Veneziano[39], M. Vesterinen[11],
B. Viaud[7], D. Vieira[2], M. Vieites Diaz[37], X. Vilasis-Cardona[36,o], V. Volkov[32], A. Vollhardt[40],
D. Volyanskyy[10], D. Voong[46], A. Vorobyev[30], V. Vorobyev[34], C. Voß[63], J.A. de Vries[41],
R. Waldi[63], C. Wallace[48], R. Wallace[12], J. Walsh[23], S. Wandernoth[11], J. Wang[59], D.R. Ward[47],
N.K. Watson[45], D. Websdale[53], A. Weiden[40], M. Whitehead[48], G. Wilkinson[55,38], M. Wilkinson[59],
M. Williams[38], M.P. Williams[45], M. Williams[56], T. Williams[45], F.F. Wilson[49], J. Wimberley[58],
J. Wishahi[9], W. Wislicki[28], M. Witek[26], G. Wormser[7], S.A. Wotton[47], S. Wright[47], K. Wyllie[38],
Y. Xie[61], Z. Xu[39], Z. Yang[3], J. Yu[61], X. Yuan[34], O. Yushchenko[35], M. Zangoli[14],
M. Zavertyaev[10,b], L. Zhang[3], Y. Zhang[3], A. Zhelezov[11], A. Zhokhov[31], L. Zhong[3], S. Zucchelli[14].

1 *Centro Brasileiro de Pesquisas Físicas (CBPF), Rio de Janeiro, Brazil*
2 *Universidade Federal do Rio de Janeiro (UFRJ), Rio de Janeiro, Brazil*
3 *Center for High Energy Physics, Tsinghua University, Beijing, China*
4 *LAPP, Université Savoie Mont-Blanc, CNRS/IN2P3, Annecy-Le-Vieux, France*
5 *Clermont Université, Université Blaise Pascal, CNRS/IN2P3, LPC, Clermont-Ferrand, France*
6 *CPPM, Aix-Marseille Université, CNRS/IN2P3, Marseille, France*
7 *LAL, Université Paris-Sud, CNRS/IN2P3, Orsay, France*
8 *LPNHE, Université Pierre et Marie Curie, Université Paris Diderot, CNRS/IN2P3, Paris, France*
9 *Fakultät Physik, Technische Universität Dortmund, Dortmund, Germany*
10 *Max-Planck-Institut für Kernphysik (MPIK), Heidelberg, Germany*
11 *Physikalisches Institut, Ruprecht-Karls-Universität Heidelberg, Heidelberg, Germany*
12 *School of Physics, University College Dublin, Dublin, Ireland*
13 *Sezione INFN di Bari, Bari, Italy*
14 *Sezione INFN di Bologna, Bologna, Italy*
15 *Sezione INFN di Cagliari, Cagliari, Italy*
16 *Sezione INFN di Ferrara, Ferrara, Italy*
17 *Sezione INFN di Firenze, Firenze, Italy*
18 *Laboratori Nazionali dell'INFN di Frascati, Frascati, Italy*
19 *Sezione INFN di Genova, Genova, Italy*
20 *Sezione INFN di Milano Bicocca, Milano, Italy*
21 *Sezione INFN di Milano, Milano, Italy*
22 *Sezione INFN di Padova, Padova, Italy*
23 *Sezione INFN di Pisa, Pisa, Italy*
24 *Sezione INFN di Roma Tor Vergata, Roma, Italy*
25 *Sezione INFN di Roma La Sapienza, Roma, Italy*
26 *Henryk Niewodniczanski Institute of Nuclear Physics Polish Academy of Sciences, Kraków, Poland*
27 *AGH - University of Science and Technology, Faculty of Physics and Applied Computer Science, Kraków, Poland*

28 *National Center for Nuclear Research (NCBJ), Warsaw, Poland*

29 *Horia Hulubei National Institute of Physics and Nuclear Engineering, Bucharest-Magurele, Romania*

30 *Petersburg Nuclear Physics Institute (PNPI), Gatchina, Russia*

31 *Institute of Theoretical and Experimental Physics (ITEP), Moscow, Russia*

32 *Institute of Nuclear Physics, Moscow State University (SINP MSU), Moscow, Russia*

33 *Institute for Nuclear Research of the Russian Academy of Sciences (INR RAN), Moscow, Russia*

34 *Budker Institute of Nuclear Physics (SB RAS) and Novosibirsk State University, Novosibirsk, Russia*

35 *Institute for High Energy Physics (IHEP), Protvino, Russia*

36 *Universitat de Barcelona, Barcelona, Spain*

37 *Universidad de Santiago de Compostela, Santiago de Compostela, Spain*

38 *European Organization for Nuclear Research (CERN), Geneva, Switzerland*

39 *Ecole Polytechnique Fédérale de Lausanne (EPFL), Lausanne, Switzerland*

40 *Physik-Institut, Universität Zürich, Zürich, Switzerland*

41 *Nikhef National Institute for Subatomic Physics, Amsterdam, The Netherlands*

42 *Nikhef National Institute for Subatomic Physics and VU University Amsterdam, Amsterdam, The Netherlands*

43 *NSC Kharkiv Institute of Physics and Technology (NSC KIPT), Kharkiv, Ukraine*

44 *Institute for Nuclear Research of the National Academy of Sciences (KINR), Kyiv, Ukraine*

45 *University of Birmingham, Birmingham, United Kingdom*

46 *H.H. Wills Physics Laboratory, University of Bristol, Bristol, United Kingdom*

47 *Cavendish Laboratory, University of Cambridge, Cambridge, United Kingdom*

48 *Department of Physics, University of Warwick, Coventry, United Kingdom*

49 *STFC Rutherford Appleton Laboratory, Didcot, United Kingdom*

50 *School of Physics and Astronomy, University of Edinburgh, Edinburgh, United Kingdom*

51 *School of Physics and Astronomy, University of Glasgow, Glasgow, United Kingdom*

52 *Oliver Lodge Laboratory, University of Liverpool, Liverpool, United Kingdom*

53 *Imperial College London, London, United Kingdom*

54 *School of Physics and Astronomy, University of Manchester, Manchester, United Kingdom*

55 *Department of Physics, University of Oxford, Oxford, United Kingdom*

56 *Massachusetts Institute of Technology, Cambridge, MA, United States*

57 *University of Cincinnati, Cincinnati, OH, United States*

58 *University of Maryland, College Park, MD, United States*

59 *Syracuse University, Syracuse, NY, United States*

60 *Pontifícia Universidade Católica do Rio de Janeiro (PUC-Rio), Rio de Janeiro, Brazil, associated to* 2

61 *Institute of Particle Physics, Central China Normal University, Wuhan, Hubei, China, associated to* 3

62 *Departamento de Fisica , Universidad Nacional de Colombia, Bogota, Colombia, associated to* 8

63 *Institut für Physik, Universität Rostock, Rostock, Germany, associated to* 11

64 *National Research Centre Kurchatov Institute, Moscow, Russia, associated to* 31

65 *Yandex School of Data Analysis, Moscow, Russia, associated to* 31

66 *Instituto de Fisica Corpuscular (IFIC), Universitat de Valencia-CSIC, Valencia, Spain, associated to* 36

67 *Van Swinderen Institute, University of Groningen, Groningen, The Netherlands, associated to* 41

a *Universidade Federal do Triângulo Mineiro (UFTM), Uberaba-MG, Brazil*

b *P.N. Lebedev Physical Institute, Russian Academy of Science (LPI RAS), Moscow, Russia*

c *Università di Bari, Bari, Italy*

d *Università di Bologna, Bologna, Italy*

e *Università di Cagliari, Cagliari, Italy*

f *Università di Ferrara, Ferrara, Italy*

g *Università di Urbino, Urbino, Italy*

^{h} Università di Modena e Reggio Emilia, Modena, Italy

^{i} Università di Genova, Genova, Italy

^{j} Università di Milano Bicocca, Milano, Italy

^{k} Università di Roma Tor Vergata, Roma, Italy

^{l} Università di Roma La Sapienza, Roma, Italy

^{m} Università della Basilicata, Potenza, Italy

^{n} AGH - University of Science and Technology, Faculty of Computer Science, Electronics and Telecommunications, Kraków, Poland

^{o} LIFAELS, La Salle, Universitat Ramon Llull, Barcelona, Spain

^{p} Hanoi University of Science, Hanoi, Viet Nam

^{q} Università di Padova, Padova, Italy

^{r} Università di Pisa, Pisa, Italy

^{s} Scuola Normale Superiore, Pisa, Italy

^{t} Università degli Studi di Milano, Milano, Italy

† Deceased